ALLOYING AND HEAT TREATMENT OPTIMIZATION OF Fe/Cr/C STEELS FOR IMPROVED MECHANICAL PROPERTIES

Contents

ALLOYING AND HEAT TREATMENT OPTIMIZATION OF Fe/Cr/C STEELS FOR IMPROVED MECHANICAL PROPERTIES

Mehmet Sarikaya

Materials and Molecular Research Division
Lawrence Berkeley Laboratory
and
Department of Materials Science and Minerial Engineering
University of California
Berkeley, California 94720

ABSTRACT

The effects of alloying elements and heat treatments on the microstructural changes and strength-toughness properties were investigated in optimization of vacuum melted Fe/Cr/C base steels.

The structure of the steels in the as-quenched conditions consisted of highly dislocated autotempered lath martensite (strong phase) and thin continuous interlath films of retained austenite (tough phase). It has been emphasized again that the mechanical properties of the steels are sensitive to the amount and the stability of retained austenite. To increase the stability of retained austenite in the as-quenched condition 2 w/o Mn or 2 w/o Ni was added to the base steel, viz., Fe/3Cr/0.3C. Partial replacement of Cr by about 0.5 w/o Mo did not alter the beneficial microstructure. At these low values of Mo addition no beneficial influence on tempered martensite embrittlement (TME) was observed.

The steels were subjected to both conventional and nonconventional heat treatments. The latter involved single high temperature (1100°C) (for dissolving alloy carbides) or double high and low (900°C) (grain refining) austenitizing. Even in the as-quenched condition the steels had attractive mechanical properties. Double heat treatments were shown to be beneficial in further increasing the mechanical

properties. This can be attributed to smaller prioraustenite grain size and higher amounts of retained austenite. Improvements in the toughness properties were attained without detoriating the strength values by low temperature tempering at 200^{o}C. Sudden decreases in the toughness values upon higher temperature tempering were attributed to tempered martensite embrittlement (TME) and temper embrittlement (TE).

The present alloys were found to have mechanical properties superior to many commercially available more complex structural steels.

I. INTRODUCTION

A. General Introduction

It is important to produce steels which have high toughness as well as high strength values for engineering applications. To design such steels it is not practical to use various kinds and amounts of alloying elements, and employ complicated thermal or thermo-mechanical heat treatments. However, the extent of alloying additions should be such that the greatest benefit should be derived. To produce further desirable microstructural changes relatively simpler heat treatments should be applied, especially considering the economical aspects.

A program[2-5,7,10-12,21,39] on the systematic investigation of alloying elements on the microstructure and the mechanical properties of experimental steels for a decade or so led to the development of Fe/4Cr/0.35C (Refs. 7 and 20) base steels. These steels have superior strength and toughness over more complex commercial steels. In this study to make the steels more desirable, more convenient alloying additions and modifications have been made.

Since Mo has similar effects as Cr, viz., carbide former, high hardenability ability, and is more economical, Fe/Mo/C steels were designed replacing Cr completely or partly.[5,10] Lower strength-toughness combinations in these steels were attributed to the absence or very low amounts of stable retained austenite phase within the structure. In the present work, the Cr percentage was decreased to 3 w/o, and 0.5 w/o Mo was added to compensate for this decrease in Cr percentage.

By the use of sophisticated methods of high resolution electron microscopy significant observations[7-8,13-14,21,32-34,55] were made on the interlath films of retained austenite in "high strength low alloy" (HSLA) steels. It was also well established that upon tempering in the 300-500°C range, these retained austenite films are destabilized and transform into interlath carbides which are extremely deleterious to toughness.[15,21,55,56] Although the exact mechanisms of stabilization of retained austenite, and its decomposition upon tempering are not known its existence was always associated with significant improvements in the toughness.[6-9,12-14,21,32-34] Also observed were the changes in the amount and stability of retained austenite with quarternary alloying additions[3,21] and heat treatments.[8,34,39-42]

While further understanding of the influence of alloying additions, viz., Mo, Ni, Mn, to the base steel on its morphology and consequent mechanical properties constitutes the main part of this study, applications of different heat treatments to further improve the toughness-strength combinations and understanding of their effect on the microstructural changes also share another part of the aim.

For the design of the alloys for optimum properties, the following guidelines were followed:

B. Improvement of Strength and Toughness

(i) Alloying Additions

In addition to economical reasons, Cr content was decreased from its original value of 4 w/o (in the base steel)[4,21] to its present value of 3 w/o in the steels designed to avoid some undesirable microstructural features, viz., microstructural twinning[1,2,7,21,50] and formation of

large chromium carbides upon tempering.[16,27,28,45] Addition of 0.5 w/o was made to replace this loss in Cr, e.g., to retain hardenability.[17,18] The Mo decreases the diffusivity of Cr in martensite which limits the formation of carbides and their growth as it does to cementite.[16,27] Having the effect of temper resistance in retained austenite, it may limit the transformation of this phase to cementite and ferrite upon tempering, viz. it postpones "TME." Even upon higher temperature tempering it is known that cementite is replaced by a distribution of stable molybdenum carbides, i.e., the secondary hardening effect.[16,27] The Mo was also reported[22-24] to reduce the severity of temper embrittlement.

Carbon is necessary to increase strength, and it is vital to obtain retained austenite.[21,55] Higher C content impedes the autotempering ability of martensite by decreasing Ms temperature.[55] High C content (>0.35 w/o) also causes the formation of microstructural twinning.[7,21,37] So C is kept at lower values (~0.3 w/o), which compromises the maximum strength that can be attained by the martensite reaction.

Mn and Ni additions (to Alloy I and Alloy II, respectively, Table I) were made mainly to stabilize the retained austenite in the presence of C.[21,55] The 2 w/o Mn was added as this content is known to give optimum properties without changing the substructure appriciably, viz., decreasing Ms, and so decreasing autotempering ability,[21,55] inducing microstructural twinning,[2,21,37,38] accelerating cementite growth.[27,28] The Ni content was kept at 2 w/o for economical reasons. Addition of the same amounts of Mn and Ni to the alloys I and II, respectively, allows a comparison to be made in the behavior of these alloys.

(ii) Retained Austenite

It is well known[6-15,21,32-34,53-56] now that interlath films of retained austenite have the effect of increasing the toughness of steels. It was speculated that thin films of retained austenite is capable of blunting moving cracks, or causing them to branch out which increases the stress necessary for further movements of the cracks.[6-9] However, austenite should be chemically and thermally stable as well as mechanically.

(iii) Grain Refining

Yield strength and fracture toughness values[17-20] increase and DBTT decreases with a decrease in prior-austenite grain size. This also decreases the severity of embrittling constituents.[29] Once a compositionally homogeneous structure is achieved by heat treatments, grain refinement increases the amount of retained austenite.[21,55] Therefore it is necessary to have grain refinement to maintain good properties.

(iv) Substructure and Carbides

Microstructural twinning in C containing martensite[1,30-32,36,48-50] is deliterious to toughness porperties[7,21,38] in the as quenched condition. Upon tempering, twin boundary carbide precipitation occurs which is more detrimental than twinning itself.[7,21,55] The occurrence of microstructural twinning was observed to increase with increasing solute content (C,[21] Cr,[4,7,21] Ni,[2,21,27] Mn,[3,21] Mo[5,10]).[55] Therefore, to utilize the alloying elements more efficiently the total solute content should be optimized such that minimum possible amount of microstructural twinning is induced.[38]

By the uniform dispersion of small carbides both the yield strengt and toughness of the martensite increase.[16] By the changes in the alloy elements and the variations in the heat treatments, the dispersion, sha size, location, nature and crystallography of carbides in steel can be controlled.[2,3,16,21,27-28,45]

(v) Austenitizing Temperature

Higher austenitizing temperatures (>900°C) are beneficial to the mechanical properties of the steels.[8,21,40-43] By high temperature austenitizing course alloy carbides can be dissolved completely and compositionally homogeneous structure can be achieved.[8,21,42] However, a very high austenitizing temperature leads to an increase in grain size. Therefore, double austenitizing, viz., high temperature austenitizing, quenching followed by low temperature austenitizing, may be applied to obtain the benefits of both treatments.

II. EXPERIMENTAL PROCEDURE

A. Materials Preparation

Both of the alloys (Table I) were supplied by Daido Steel Company, Japan. They were vacuum induction melted into 20 lb ingots and subsequently rolled to 1 in. thick and 25 in. wide slabs. Alloys, then, homogenized at 1200°C for 24 hrs and furnace cooled. Plane strain fracture toughness and Charpy V-notch impact toughness specimens were obtained from the slabs. Round tensile specimens were obtained from 0.75 in.-diameter rods (Fig. 2). Cwmpositions of the alloys are given in Table I.

B. Heat Treatments

Basically three kinds of heat treatments were applied; heat treatments I, II and III. (They will be designated as H.T.(I), H.T(II), and H.T(III) (Fig. 3)). They involve high and/or low temperature austenitizing, quenching, and tempering. All the austenitizing treatments were carried out in a vertical tube furnace under argon atmosphere. Oversized tensiles, Charpy and K_{IC} specimens were cut from their stocks and machined to blanks. At the end of austenitizing treatment specimens were quenched in agitated oil placed under the furnace. All the tempering treatments (200°C through 600°C) were carried out by immersing the specimens into a salt pot for 1 hour and then quickly quenching into a water. Final machining was done under flood cooling to avoid heating.

C. Dilatometry

A commercial dilatometer was used to obtain the cooling and heating curves. Hence phase transformation temperatures, viz., M_s, M_f (martensite start and finish) and A_s and A_f (austenite start and finish) of the alloys were determined from these curves (Table I).

D. Mechanical Testing

(i) Tensile Testing

Round tensile specimens (Fig. 2a) with 1.25 in. gauge were tested at room temperature in a 300 Kip capacity MTS testing machine at a cross-heat speed of 0.04 in./min.

(ii) Fracture Toughness Testing

Plane strain fracture toughness values (K_{IC}) were obtained by testing standard compact tension crack line loaded toughness specimens (Fig. 2b). After each heat treatment about 0.01 in. thickness was removed from each flat surface of the K_{IC}-blanks. The thickness of the specimens conformed to the ASTM specifications[39] for plane strain condition, viz.,

$$\text{thickness} \geq 2.5\left(\frac{K_{IC}}{\sigma_y}\right)^2 \quad .$$

The 300 Kip MTS machine was again used for fatique precracking the specimens to a minimum crack length of about 0.05 in. Specimens then subsequently tested in the same machine to obtain the fracture toughness data. The orientation of crack propagation with respect to the long dimension of the bar stock is L-T.[39]

(iii) Charpy Impact Testing

Size of the standard specimen is shown in Fig. 2c. Two or three specimens were tested for each heat treatment, and data points were taken as the average of these. To determine the ductile-to-brittle transition temperature (DBTT) specimens were tested at different temperatures below and above room temperature. To obtain subzero temperatures varying proportions of liquid nitrogen and ethyl alcohol were used.

Charpy specimens were immersed in these mixtures and kept there for a sufficiently long time to attain the temperature of the both before break-in them. For above room temperature tests a water bath with thermostat was utilized.

E. Metallography

(i) Optical Metallography

Specimens for optical metallography were cut mostly from broken Charpy bars, mounted in cold-mount, abraded on silicon carbide papers down to 600 grit, and polished on 1 μm-diamond abrassive wheel. For revealing martensitic microstructure and prior austenite grain boundaries specimens were etched in 5% nital solution. For fine grained specimens an etchant of 5 gm of picric acid in 100 cc of water saturated with dodacylbenzene sulfonate was used.

(ii) Scanning Electron Microscopy and Energy Dispersive Analysis of X-Rays

An AMR-1000 scanning electron microscope at 20 kV was utilized to conduct fractographic study on Charpy specimens. An energy dispersive analysis of X-rays (EDAX) unit attached to the microscope was used to analyze the indlusions semiquantitatively.

(iii) Transmission Electron Microscopy (TEM)

Thin foils for TEM were obtained from Charpy specimens. About 20-mil thick slices were cut longitudinally from these specimens. After removing any oxide scale by cleaning, these slices were chemically thinned to about 5 mils in a solution of 4-5% HF in H_2O_2 at room temperature. Three mm-diameter discs were spark cut from these thinned slices. Discs were then carefully sanded down to about 2 mils thickness. Finally these thin foils were electropolished in a

twin-jet electropolishing apparatus at room temperature using a chromacedic acid solution made of 75 gm CrO_3, 400 ml CH_3 COOH and 21 ml distilled water. The polishing voltage varied between 40-45 volts, and that of current about 50-55 milliamers. Thin foils so obtained were kept in ethyl-alcohol for later uses. Oxide layers cover the polished surfaces of the foils for very long time storage. These layers may be removed by repolishing the foil by holding it delicately with a pair of twezers and carefully immersing it in agitated polishing solution for about a minute. Foils were then subsequently examined in JEM-7A and Phillips EM 301 electron microscopes at an accelerating voltage of 100 kV.

III. RESULTS

A. Transformation Temperatures and Heat Treatments

Martensite transformation temperatures M_s and M_f and austenite formation temperatures A_s and A_f were obtained by dilatometry. As can be noted (Table I), the M_s temperatures of the alloys are quite high, viz., 320°C for Mn and 340°C for Ni-containing steels. Although M_s temperature measurements reflect quite accurate values, M_f temperatures are only approximate.

In order to understand the influence of alloying additions on the morphology and substructure of steels a high austenitizing temperature of 1100°C was employed to dissolve any alloy carbides present within the structure.[40-42] Following austenitizing, specimens were quenched in oil to transform the austenite to martensite.

High temperature austenitizing resulted in coarse austenite grain sizes, for e.g., about 300 μm. For this reason double heat treatments, consisting of high and low temperature austenitizing (H.T.(II)), were applied to obtain the benefits of high temperature austenitizing and grain refining[39,21] (Table II). A third kind of heat treatment, H.T.(II) consisting of high and low temperature austenitizing with intermediate low temperature tempering, viz., 200°C, was utilized (Fig. 3). It was thought that low temperature tempering would result in a fine dispersion of carbides which upon subsequent low temperature austenitizing act as nucleation sites for austenite phase (Fig. 3). Also applied was the conventional heat treatment (H.T.(c), Fig. 3) to compare the results with those of the unconventionally heat treated steels.

B. Microstructural Characterization

(i) Optical Metallography

Optical metallography has been utilized to observe any variations in the apparent features of the microstructure, viz., prior austenite grain size,[46] coarse undissolved carbides, etc., with heat treatment and compositional changes. Figure 4 shows representative optical micrographs of Alloy I and Alloy II for different heat treatments. The structures are composed of martensite packets containing laths. There were no undissolved carbides in alloys subjected to either experimental single or double heat treatments.

Table II shows the variations in the prior austenite grain size with different heat treatments. This is also reflected in Fig. 4. In the single treated steels, the grain size is very large (~300 μm, Fig. 4a and 4b). In the double heat treated steels fairly small grains were observed (~30 μm, Fig. 4c and 4d). H.T.(III) produced more uniform grains of austenite (Fig. 4e and 4f).

(ii) Transmission Electron Microscopy

Characterization of microstructures by transmission electron microscopy was done on both alloys for all the heat treatments applied, viz., single heat treatment in the as quenched and quenched and tempered (200-500°C) and double heat treatments in the quenched and 200°C tempered conditions. In the following section morphological changes in the martensite substructure will be covered, and the behavior of retained austenite will be dealt with later.

a. [illegible] ture of the Alloys in the As-Quenched Condition

[illegible]rphology of martensite in these alloys is lath type (Refs. 1, [illegible]7-49,57,59). In a certain packet laths are fairly parallel

to each other. Typical examples in Fig. 5, where laths of 0.5 μm width, are seen from Mn (a) and Ni-containing steels (b).

Two very important substructural variations were observed in these alloys, viz., microstructural twinning and autotempered carbides. Although the significant part of martensite laths are heavily dislocated (Fig. 5), a small amount of $\{112\}_\alpha$ substructural twinning has been observed in both steels (Fig. 13). Amount of substructural twinning in Ni containing steel was, however, much lower than that of 5 w/o Ni containing base steel[21] and higher than Mn containing steel.

Significant amount of autotempering occurred in both of the alloys. This is more severe in Ni containing steel (Fig. 6) which may be attributed to somewhat higher Ms temperature of Alloy II (Table I). In the Mn-containing steel $\{110\}_\alpha$ widmenstatten cementite precipitation was observed. In the Ni containing steel mostly ε-carbides were present. In instances where no good diffraction pattern was obtained to identify cementite, its presence was ascertained by the widmenstatten nature of cementites which form on {110} planes of martensite. In micrographs where electron beam direction is ⟨111⟩ they appear as platelets making 120° angle to each other (refer to later pictures, viz., Figs. 7, 9, 10, 12 and 14) ε-carbide in Alloy II may be characterized by their "cross-hatched" appearance or "wavy" interface which are growing in $(121)_\alpha$ direction[2,21,26] (Figs. 6 and 24).

b. Structure of the Alloys in the Tempered Conditions

200°-Tempering. Upon 200°C tempering $(110)_\alpha$ widmenstatten cementite precipitates were observed in both alloys (Fig. 7). However, ε-carbides were still present in the Ni containing steel. The

orientation relation ship between cementite and martensite was found to obey the Bagaryatski relationship. An example is given in Fig. 7d, viz.,

$$[111]_M // [100]_C \quad \text{and} \quad (0\bar{1}1)_M // (011)_C \quad .$$

The micrographs (e) and (f) in Fig. 7 which were taken using very high magnification show carbides are precipitating on dislocations (Micrograph (e) is "Weak Beam Dark Field" of $g_{01\bar{1}}$ of martensite). The cementite precipitates upon this temperature tempering were 0.3-0.5 μm long and 200 to 500 Å wide.

300°C Tempering. The amount of intralath carbide precipitation greatly increased following 300°C tempering. While new carbides start forming existing ones grow further (Fig. 8). Following 300°C ε-carbides in Ni containing steel were replaced by widmenstatten cementite (Fig. 9). No spheroidization of carbides observed in any of the alloys tempered at this temperature. Figures 8 and 9 also show carbides forming on the microstructural twins, in Alloy I and Alloy II respectively, which were formed during quenching.

400°C Tempering. Upon 400°C tempering carbides continue to grow. Extensive $\{110\}_\alpha$ widmenstatten cementite precipitation has been observed (Fig. 10). Spheroidization seems to be just starting. This is evident in Fig. 11, where carbides are shown without arrows. Figure 12 taken from the Ni containing steel shows both grown widmenstatten cementite plates and spheroidized cementites of globular appearance. Morphological changes taking place by increasing the tempering temperature from 200°C through 400°C can be distinguished by carefully examining the BF micrographs in Fig. 13 (from Alloy II).

500°C Tempering. At this tempering range, spheroidization is much advanced. Figure 14 shows coarse spheroidized cementite in the Ni containing steel. Carbides precipitating within laths and on microtwins grow further. Even at this temperature widmenstatten cementite still exists (Fig. 14). No alloy carbides could be identified even upon this temperature tempering.

c. Behavior of Retained Austenite

After its first identification in Fe/Cr/C experimental steel[7] with the use of transmission electron microscopy, considerable attention has been given to retained austenite occurring in lath martensitic H.S.L.A. steels of various compositions.[6-8,12,21,32-34,55,60] Although the bulk Ms and Mf temperatures of the steels are well above room temperature, viz., Ms > 300°C, significant amounts (~4%) of retained austenite films were found at the lath boundaries (Fig. 15).

The occurrance and stability of this phase are important in determining the mechanical properties of steel. And yet its existence is essential to explain some of the mrophological and crystallographical changes in the lath martensitic structure. In the following section the electron microscopical identification of retained austenite, and its distribution and orientation relationship with martensite will be discussed.

Electron Microscopical Observations. Extreme care should be encountered in the identification of an austenite reflection in a diffraction pattern which contains overlapping diffraction patterns from several laths and different carbides.[55] As has been suggested[44,55] for dark field imaging of retained austenite $(002)_\gamma$ reflection was used

(Figs. 15 and 16). In Fig. 16, which is from Alloy II in the as-quenched condition, micrograph (b) was taken by using $(00\bar{2})_A$ reflection and (c) by using $(020)_M$ reflection which show changes of contrast from retained austenite to martensite. Retained austenite phase in the as-quenched condition is in the form of very thin (150-200 Å) and continuous films between the martensite laths (Fig. 15). According to the TEM observations there was no difference in the amount of retained austenite in either of the alloys.

Orientation Relationships. Almost always both K-S (Kurdjumov-Sachs) and N-W (Nishiyama-Wesserman) orientation relationships were observed together between martensite and austenite within the same packet in both of the alloys (Figs. 16 and 21). Considering the diffraction pattern in Fig. 16e, we see that there are two martensite zones, viz., $[100]_\alpha$ and $[111]_\alpha$, and single austenite zone, viz. $[110]_\gamma$. Taking into account only one martensite crystal variant at a time, the $[111]_\alpha$ and $[110]_\gamma$ combination results in K-S relation, and $[100]_\alpha$ $[110]_\gamma$ combination results in N-W relation. These orientation relations have been observed in medium carbon experimental steels between austenite and lath martensite by other workers.[21,43,55,58,60] Thomas and Rao[57] concluded that the dominant orientation relation is K-S or N-W depending on the composition of the steel. In the present investigation both of the orientation relationships occurred frequently, and most often together, in both of the alloys.

Distribution of Retained Austenite. A significant variation in the amount of retained austenite within a given specimen in the as-quenched and 700°C tempered condition has been observed. This is explained by the influence of adjacent lath orientations on the occurrence of

retained austenite.[60] In Fig. 17 three impinging packets, viz., A, B, and C, can clearly be seen. No retained austenite was found in the packet B containing laths 1 through 5. These laths are twin related,[57,59] hence they are self accommodating. Note that the interface plane for these twin related laths is $\{110\}_M$. So for $\{110\}_M$ $\langle 111\rangle_M$ twinning shear, in the [111] orientation identical SAD pattern are obtained from the matrix and the twin (Fig. 17, SAD patterns). In the same figure, in the packets A and C, surrounding the central packet B, the laths are not twin related. Indeed the detailed analysis of these packets showed the presence of retained austenite.

Thermal Stability By tempering the steels the stability of retained austenite was changed. Upon 200°C tempering, it was stable in both alloys (Figs. 21, 22 and 23). Following 300°C tempering, while it was still stable in the Ni-containing steels, there was no retained austenite present in the Mn containing steel. Instead, as a result of the decomposition of austenite, coarse carbides were precipitated at the lath boundaries (Fig. 18). Following 400°C tempering, the same transformation occurred which resulted discontinuous coarse stringers of carbides at the same sites in both Ni containing (Fig. 19; also note Fig. 11 identified by arrows) and the Mn containing steels (Fig. 20, and also, Fig. 11). These interlath cementite particles continued to precipitate after 500°C tempering (Fig. 14). This figure also shows interlath cementite precipitation concurrent with the spheroidization of intralath cementite.

d. Structure of Modified Heat Treated Steels

By the application of H.T.(II) (Fig. 3), for grain refining, almost the same type of morphological appearances similar to those

seen following single heat treatment were observed. Structures were examined after 200°C tempering. Fairly parallel lath morphology of martensite is evident in the microstructures, for e.g., Fig. 21 (from Alloy I). Only cementite precipitation occurred in the Mn containing alloy. On the other hand, ε-carbide precipitation was dominant in the Ni containing steel.

Martensite lath boundaries were again decorated by narrow films of retained austenite (Fig. 22). The overall amount of retained austenite seemed to be higher than in single treated steel, as it is obvious in Fig. 23.

Microstructures of the steels upon application of H.T.(III) were essentially the same. However, more extensive carbide precipitation was observed (for e.g., Fig. 24 from Ni-containing steel).

C. Mechanical Properties

Mechanical properties of both of the steels are tabulated in Table III and Table IV for single and double treated steels, respectively.

(i) Tensile Properties

As shown in Fig. 25, hardness varies as a function of tempering temperature for single treated steels. The temper resistance for the Ni containing steel is superior to the Mn containing alloy in the range 300-500°C. The same type of behavior is also seen in Fig. 25 where both YS and UTS show a levelling-off behavior in the same temperature range in both alloys. In the as-quenched condition yield strength values of both alloys are about 200 ksi, which slightly increase upon 200°C tempering. The UTS values always decrease. Both YS and UTS decrease as tempering temperature continues to increase. A rapid decrease occurs in the strength of both alloys following 500 to 600°C

tempering. Elongation values generally increase with tempering temperature (Table III).

(ii) Fracture Properties

For measuring fracture properties both plane strain fracture toughness (K_{IC}) and Charpy V-notch impact toughness tests were conducted. The data are tabulated in Tables III and IV. Because of a limited amount of material available, K_{IC} tests were applied to both alloys only in the as quenched and 200°C tempered conditions. However, Charpy tests were run through all tempering temperatures, viz., 200°C through 600°C (Fig. 27).

Somewhat low K_{IC} values for both of the steels in the as-quenched condition were improved greatly by tempering at 200°C contaminant with slight increase in yield strength (Fig. 28). In fact this is the condition for the best properties for the single treated steels.

The most dramatic variations occur in the CVN-Impact values with the tempering temperature (Fig. 27). Following 200°C tempering impact values increases significantly as compared to the values in the as-quenched condition. This is the same type of trend seen in K_{IC} test. Upon higher temperature tempering values start decreasing. A very sharp decrease occurs in the Mn containing steel after 300°C tempering. This is due to TME.[15,21,22,26,55,56] A second minimum occurs for the same steel upon 500°C tempering due to TE.[15,16,21,23,24,55,56] However, in the Ni containing steel only one minimum occurs following 400°C tempering at higher values of energy. This is probably due only to the TME. Both alloys show sharp increases in the impact energy values following 600°C tempering (Fig. 27).

Charpy tests were conducted at different test temperatures in order to obtain ductile to brittle transition temperature (DBTT) (Fig. 2[illegible]). The DBTT range is much wider and there is no definite upper-shelf energy value for Mn containing alloy. However, for Ni containing alloy, the range is narrower, viz., -150 to 50°C, and impact energy has an upper shelf of about 30 ft-lb. It should be remembered, though, that the DBTT depends on the criterion used to determine it.

(iii) Changes in the Mechanical Properties with Heat-Treatment Modifications

A general trend of increase in K_{IC} and CVN-impact energy values occur with very slight or no change in strength values following the experimental double treatments (Fig. 28). By the application of single high temperature austenization (H.T.(I)) steels show significantly high Charpy values compared to the conventional low temperature austenitization H.T.(C)(Fig. 28a), while yield strengths do not change notably. By the application of double heat treatments, viz., H.T.(II) and H.T.(III) further increases in the Charpy values occur (Fig. 28a). The same type of improvements are apparent in the K_{IC} values of the Mn containing steel with the same order of modifications in the heat treatments. This is not quite true for the Ni containing steel (Fig. 28b). Following [illegible]°C tempering after austenitizing treatment(s), almost always significant improvements occur in the fracture values, while slight increases in the strength values are also apparent.

D. Fractography and Particle Characterization

To study the failure modes of fracture, specimens were examined in scanning electron microscope. For this purpose broken Charpy specimens were used, since CVN-impact energy values showed the most dramatic

variations with alloying and heat treatment.

Fracture surfaces of the single treated steels in the as-quenched and 200°C tempered conditions are shown in Fig. 30. Both alloys show highly ductile dimpled rapture fracture surfaces in the as-quenched condition. Dimples are much larger and some quasicleavage occur in Mn containing steel (Fig. 30a). In the 200°C tempering condition fracture modes are similar to those in the as-quenched condition. Here dimples are shallower and their sizes are smaller (Fig. 30c and Fig. 30d). Sharp changes in the fracture mode occur after 300°C tempering, especially in the Mn-containing steel. Figures 31a and 32a show brittle quasi-cleavage fracture with parallel ridges of the order of lath widths and deep cracks on the fracture surface of Alloy I. This is probably due to TME. Although this is not severe in the Ni containing steel, following 400°C tempering almost the same type of fracture surface appearence is evident in Figs. 31d and 32b, that is, a fracture which is intergranular with respect to prioraustenite grains but intergranular with respect to individual laths. Tempering at 500°C mostly brittle intergranular fracture together with some-quasicleavage dominate the fracture mode in Alloy I (Fig. 33a). This kind of intergranular embrittlement is associated with the segragation of some impurity elements to the preaustenite grain boundaries which lower the intergranular cohesion.[15,16,23,24,26,55] Upon 600°C tempering intergranular appearance of the fracture surface in Alloy I becomes more complete and cracks between grains are more severe (Fig. 33c--note the seperation between the grains). In the Ni-containing steel following 500 and 600°C tempering, ductile dipled

rupture dominates the fracture mode (Fig. 33b and Fig. 33d).

A ductile fracture mode was operative in both of the alloys upon application of double heat treatments. Fracture surfaces containing mostly dimples (smaller in Alloy II) are clear in Fig. 34a and Fig. 34b. Figures 34c and 34d show relatively brittle fracture surfaces consisting of shallow and deep dimples quasicleavage and deep cracks in the conventionally treated alloys.

Although the alloys were vacuum melted there were probably still residual elements present in the structure which sometimes appear as inclusions. To characterize the inclusions qualitatively an X-ray energy dispersive analysis unit attached to the scanning electron microscope was used. Inclusions, almost always seen in the Mn containing steel, were mostly situated at dimples. Figure 35a and Fig. 35c illustrate various types of inclusions observed in Alloy I following 200°C tempering with the corresponding X-ray energy spectrums. Spherical and rather smaller, viz., 1-2 μm diameter, inclusions were characterized as (FeMn)S particles with varying Fe and Mn peaks, Figs. 35a and 35b. Other inclusions were larger, viz., 3-5 μm diameter, and had rather irregular shape gave Al-peak which were probably due to Al_2O_3 inclusions.

IV. DISCUSSION AND SUMMARY

A. Variations in the Microstructure Due to Composition and Heat Treatment

(i) As-Quenched Steels; Martensite Substructure and Retained Austenite

The morphology of the martensite in both of the steels was basically heavily dislocated lath martensite[1-4,21,28,48-51,57,59] (Figs. 5,17). However, sometimes substructural twinning was observed (Fig. 13) which mainly affected the toughness of the steels.[7,21] The factors contributing the twinning have been discussed by various authors. Low Ms temperature[1,38] together with increasing composition of C and other alloying elements (Cr,[7,21] Mn,[2,3,21], Ni[2,37,21] Mo[5,10,)55] promote the amount of twinning.[38] Most often $\{112\}_\alpha$ twinning was observed. The amount of microtwinning was low due to somewhat low C and overall alloy contents, and high M_s temperatures of the alloys. Nevertheless, microstructural twinning were still present which upon tempering acted preferential precipitation sites for carbides (Figs. 8 and 9). This reduces toughness by providing easy crack propagation.

Retained austenite, in the form of continuous, thin (200-250 Å), inter lath films, was one of the main features in the structure of the steels investigated (Fig. 15). The existence of this high temperature phase at room temperature in steels having bulk M_s and M_f temperatures well above room temperature was attributed to several mechanisms. Interstitial C has been shown to have significant influence in obtaining retained austenite.[21] In his work, Rao[21] has outlined the stabilization mechanisms as follows; (i) chemical stabilization[28] due to the partitioning of C between martensite and austenite which lowers the local

M_s in γ;[33] (ii) thermal stabilization where C atoms form dislocation atmospheres especially at the martensite/austenite interphase which reduces the interphase motion; (iii) mechanical stabilization due to plastic deformation in austenite during shear transformation.[47,50] The effect of other alloying elements, viz., Mn, Ni, was believed to dictate the amount of retained austenite through their interaction with C. Almost equal amounts of retained austenite were obtained by the same heat treatments in Alloy I and Alloy II (Figs. 21 and 22) due to the similar behavior of Mn and Ni in stabilizing austenite. Also, they have M_s temperatures very close to each other (Table I).

Significant variations in the amount of retained austenite in a given specimen has been attributed to the relative orientations of the adjacenent laths stabilizing the austenite.[60] Thomas and Rao[57] reported that a group of laths (3 to 5) in the same packet are so oriented with respect to each other such that a reference shear vector undergoes a 180° rotation. In that group, this result in the minimization of overall shape deformation and its accommodation over the group of laths. It is also possible that adjacent laths are twin related.[57] In this case a 180° rotation is performed in a single step. In Fig. 21, the combination of adjacent lath orientations is $(111)_M$ and $(100)_M$. Hence adjacent laths are rotated by about 55°. This is far less than 180° necessary to achieve efficient accommendation of shape strain. Therefore it is possible that the surrounding austenite films undergo deformation to provide the necessary accommodation, and hence, they are mechanically stabilized. However, in Fig. 17 where in the central packet B the laths (1 through 5) are twin related. Hence they are self accommodating. Therefore no

retained austenite was present in this region.

Both K-S and N-W orientation relationships between martensite and austenite phases were observed frequently, and often together, in both of the alloys. They are

$$(110)_M // (111)_A$$

$$[1\bar{1}1]_M // [1\bar{1}0]_A \quad \text{for} \quad \text{K-S},$$

and

$$(110)_M // (111)_A$$

$$[001]_M // [1\bar{1}0]_A \quad \text{for} \quad \text{N-W}$$

as shown in the carefully indexed diffraction pattern of Fig. 21c. Most frequently, both orientation relationships were occurring alternatingly amongst the laths of the same packet (Figs. 16 and 21). It has been hypothesized that[57] the two orientation relations give better flexibility in terms of increased varient available during martensite nucleation.[21,59]

Fine preaustenite grain size affects the stability of retained austenite.[21] The amount of retained austenite in double treated steels was higher than in single treated steels (especially pronounced in Fig. 23).

(ii) Tempered Conditions

Complexity of the events occurring during tempering of these alloys is obvious from the complexity of the compositions of the alloys compared to relatively simpler ternary systems extensively studied by various investigators.[16,27,28] Nevertheless, an attempt will be made here to correlate the microstructural variations observed during tempering with the behavior of C and other alloying elements.

Due to the high M_s temperature of the steels extensive amounts of autotempering are evident (Fig. 6). During quenching, after the formation of martensite, C atoms have enough time to redistribute themselves around individual dislocations and cell walls,[28] initial stage of tempering. These clusters then grow to form carbides following low temperature tempering (Fig. 7e and Fig. 7f), first stage of tempering. Alloying elements Mn and Ni have significant differences in influencing the carbide formation and stability. Mn together with existing Cr in the solution can stabilize cementite by replacing Fe in Fe_3C.[21] However, Ni destabilize cementite by promoting graphitization.[28,21] The resulting behavior in Alloy II is a consequent compromise between the opposing tendencies of Cr and Ni in stabilizing cementite. These effects can be seen in 200°C tempered condition. Predominantly ε-carbides (Figs. 6 and 24) and small amount cementite form in Ni containing steel. While only cementite formation was observed in Mn-containing steel (Fig. 7). Various orientation relations were observed between ε-carbide and martensite. A specific one shown in the SAD pattern of Fig. 34 is;

$$(0\bar{1}1)_M // (\bar{2}204)_C$$

$$[100]_M // [5\bar{1}\bar{4}3]_C$$

Following 300°C tempering cementite formation is dominant in both of the steels (Figs. 12 and 13); forth stage of tempering. $(110)_\alpha$ widmenstatten array of Fe_3C plates is obvious in all of the micrographs showing cementite precipitation (Figs. 8-14). As tempering temperature is increased this plate shaped Fe_3C gradually spheroidizes to reduce the

steel (Fig. 19). The decomposition reaction was speculated to be upper bainitic.[21,55] From the diffraction pattern in Fig. 20c the orientation relationship between matrix and interlath cementite is;

$[011]_M // [01\bar{1}]_C$

$[311]_M // [01\bar{1}]_C$

$[01\bar{1}]_M // (022)_C$

This is not Bagaryatski orientation relationship between ferrite and carbide. Hence these carbides precipitate directly from austenite.[3,24,48] Formation of stringers of coarse carbides at the lath boundaries provide easy crack paths. This causes a drop in toughness (Fig. 27). Hence the fracture is transgranular with respect to prior austenite, but it is intergranular with respect to individual laths (Figs. 31 and 32). The formation and growth of cementite are important in cementite precipitation from austenite. Mo limits the formation and growth of cementite in steel. But apparently this influence of Mo was not effective in Mn containing steel due may be to the small Mo content, viz., 0.5 w/o. However, the fact that TME, or also known as "500°F embrittlement," occurs at higher tempering temperatures in Ni containing steel is because Ni is a graphitizing element. Hence in the presence of Ni, concurrent with Mo, higher temperatures are necessary to transform retained austenite to $\alpha + Fe_3C$.

At higher temperature tempering, viz., 500°C, a second embrittlement, called TE, occurred in Mn containing steel. This is generally believed to be caused by the segregation of impurities to the prior austenite grain boundaries, which then lose cohesion. Hence intergranular fracture occur (Figs. 33a and 33b). Mo is known to decrease the severity[22,24]

of this segregation. But the susceptibility of a steel to TE is enhanced by the co-segragation of alloying elements, like Cr and Mn.[28] TE, together with TME, decreases toughness values even further in Mn containing steel (Fig. 27). However, still, the presence of Mo in the steel seems to decrease the synergistic effects of TME and TE by increasing the Charpy values to higher levels. There was no significant change in the failure mode upon high temperature tempering of the Ni-containing steel. Predominantly ductile dimpled rupture and quasicleavage fracture mode is evident in Fig. 33b and Fig. 33d. Therefore TE does not occur in Alloy II. This is also reflected in Fig. 27 where only one minimum occurs for Ni-containing steel.

B. Summary of the Correlation of Mechanical Properties with Microstructural Changes

By the application of high temperature austenitization (1100°C) coarse alloy carbides were dissolved in the steels and compositionally homogeneous austenite phase was obtained. Hence more reasonable correlation of mechanical properties with the microstructural variations could be made. Even in the as-quenched conditions mechanical properties are very good (Table II and IV, Figs. 26, 27, and 28). Somewhat lower strength values may be attributed to the slightly lower C content of the alloys investigated (C ~ 0.26%) than that in the base steel (C ~ 0.35%).[21] Following tempering at 200°C a small increase in yield strength (Fig. 36), but significant improvements in CVN-impact energy and K_{IC} values were obtained (Fig. 27). These increases may be due to newly formed, very small carbides which increase the flow stress in martensite (Fig. 7e and Fig. 7f). High toughness values in the as-quenched and 200°C tempered conditions

surface energy.[16,28] However as compared to the quaternary Fe/4Cr/0.3C steels, no spheroidization was observed following 300°C tempering in these steels containing 0.5 w/o Mo. Mo is known to be a strong carbide forming element.[16-19,27,28] It reduces the growth rate of cementite at low temperature tempering range, or with other carbide formers, here Cr, and replaces Fe_3C following higher temperature tempering (>500-600°C). Hence spheroidization processes became effective after 400°C tempering. As shown in Fig. 11b and Fig. 11d one or more spheroids form on an existing cementite platelet. Following 400 and 500°C tempering very fine scale precipitation of carbides were observed (Fig. 12b). Although from the diffraction patterns obtained, the identification of these carbides was not possible they may be speculated as possibly $(MoCr_2)_C$ (Ref. 28) or M_7C_3 (Ref. 16) carbides nucleating on the dislocations. Upon higher temperature tempering cementite platelets continues to grow and large spheroids form (Fig. 14, sites A and C, respectively).

Embrittlement During Tempering. Both "Tempered Martensite Embrittlement" (TME)[15,21,22,55,56] and "Temper Embrittlement" (TE)[15,16,22-24] were observed. These phenomena and observed temperatures may be explained in conjunction with the behavior of retained austenite, carbide formation, and segregation of residual elements.

Retained austenite was stable following 200°C tempering in both alloys (Figs. 21, 22 and 23). But following 300°C tempering austenite decomposes in Mn containing alloy (Fig. 18). The same type of transformation occurs following 400°C tempering in Ni-containing

are due to stable austenite films at the martensite lath boundaries. (Refs. 6,7,12-14,21,33-35,55). This austenite phase is very tough and break the continuity of brittle martensite phase. It acts as barriers to the moving cracks; it either stops them or causes them to branch out.[9] As a result more stress must be applied for cracks to overcome this barrier. It may also transform into martensite by TRIP mechanisms.[52] Retained γ also prevents lath boundary carbide precipitation. High toughness values in both of the alloys in the as-quenched and 200°C tempered conditions were also reflected in the SEM fractographs which show mainly ductile dimpled rupture (Fig. 30). Toughness values in Mn containing steel are higher than in Ni containing steel. This is, probably due to the differences in substructural twinning and inclusions in the steels.

In the temperature range of 300-500°C, a levelling of behavior is observed in the tensile strength vs tempering temperature plots (Fig. 26). Before this temperature regime ε-carbide to cementite transformation takes place. Increasing the temperature accelerates the growth of cementite. In the later stages carbides start spheroidizing. However, due to carbide formers in the structure, they are not free to grow. All these processes consume C. Events occurring in the structures in the 300-500°C temperature range were discussed before, in conjunction with TME and TE. Upon higher temperature tempering ($T \geq 500°C$) strength values continue to decrease (Fig. 26). This is due to recovery and also lower C content in the solution.

High temperature austenitization, in addition to eliminating undissolved coarse carbides, also resulted in coarse austenite grain size (Fig. 4). Charpy impact toughness is especially sensitive to prior-austenite grain size. Also evident is that grain refining increases the percentage of retained austenite (Fig. 23). Upon application of H.T.(II), improvements in the fracture and impact properties can be seen in Figs. 28a and 28b. However, strength values are slightly lower due to the increased amount of retained austenite. Overall effect of uniform and small grains of prior austenite and dissolution of carbides following H.T.(III) is reflected as further increase in toughness values (Figs. 28a and 28b). By the application of conventional heat treatment, viz., H.T.(C) (Fig. 3), steels showed brittle behavior (Figs. 38b and 48), because of much lower amount of retained austenite and the presence of larger alloy carbides.

By rearrangement and additions of the alloying elements and the applications of unconventional heat treatments desired microstructure can be obtained (Fig. 1). As a result of the overall optimization the experimental alloys have superior strength and toughness combinations compared to the equivalent commercial alloys (Figs. 36a and 36b).

CONCLUSIONS

From this investigation of microstructure and mechanical properties of Fe/3Cr/0.3C/0.5Mo with 2 Mn or 2 Ni steels, which were unconventionally heat treated, the following conclusions can be drawn:

i) Decreasing Cr content from its original value of 4.0 w/o to its present value of 3.0 w/o, and addition of 0.5 w/o Mo to the base steel do not change the microstructural features and mechanical properties significantly. As a consequence, a combination of high strength and high toughness was maintained.

(ii) The 0.5 w/o Mo addition was not enough to postpone TME to higher temperatures. But, its presence decreased the severity of TE.

(iii) There is a strong evidence to suggest that the distribution of retained austenite in the as-quenched condition can be accounted for by the relative orientation of adjacent laths. No retained austenite was found between twin related laths. However, extensive amount of it was present at the lath boundaries when the laths were not twin related (mechanical stabilization).

(iv) The fact was again reinforced that Mn-containing alloy is very sensitive to the decomposition of retained γ.

(v) In Alloy II, decreasing Ni content from its original value[21] of 5.0 w/o to its present value of 2.0 w/o caused a significant decrease in the amount of microtwinning, but slight decrease in the amount of retained austenite was also evident.

(vi) It was possible to increase the toughness properties by the application of unconventional heat treatments, viz., H.T.'s(I), (II), and (III), without deteriorating the strength properties.

ACKNOWLEDGEMENTS

The author wishes to extend his sincere appreci .ion to Professor Gareth Thomas for his support and buidance throughout the course of this investigation. Deep appreciation is extended to Dr. B. V. Narasimha Rao for his patient instruction, encouragement and many helpful discussions.

The author wishes to thank Professors Iain Finnie and J. W. Morris, for their critical appraisals of the manuscript.

Financial support was given by Scientific and Technical Research Council of Turkey.

This work was done under the auspices of the Division of Materials Science, Office of Basic Energy Sciences, U. S. Department of Energy through the Materials and Molecular Research Division of the Lawrence Berkeley Laboratory under Contract No. W-7405-ENG-48.

REFERENCES

1. G. Thomas: Met. Trans., 1972, 2, p. 2373.
2. S. K. Das and G. Thomas: Trans. ASM, 1969, 62, p. 659.
3. D. H. Huang and G. Thomas: Met. Trans., 1971, 2, p. 1587.
4. M. Raghavan and G. Thomas: Met. Trans., 1971, 2, p. 3433.
5. I. Lin Cheng and G. Thomas: Met. Trans., 1972, 3, p. 503.
6. V. F. Zackay, E. R. Parker, and W. E. Wood: Proc. 3rd Intern. Conf. on Strength of Metals and Alloys, Inst. of Metals, London, 1973, 1, p. 175.
7. J. McMahon and G. Thomas: Proc. 3rd Intern. Conf. on Strength of Metals and Alloys, Inst. of Metals, London, 1973, 1, p. 180.
8. G. Y. Lai, W. E. Wood, R. A. Clark, V. F. Zackay and E. R. Parker: Met. Trans., 1974, 5, p. 1663.
9. D. Webster: Met. Trans. 1971, 2, p. 2097.
10. R. A. Clark and G. Thomas: Met. Trans., 1975, 6A, p. 969.
11. B. V. N. Rao and G. Thomas: Mat. Sci. and Eng., 1975, 20, p. 195.
12. G. Thomas: Batelle Colloquium on Fundamental Aspects of Structural Alloy Design, R. I. Jaffee and B. A. Wilcox, eds., Plenium Publ. Co., 1977.
13. V. F. Zackay and E. R. Parker: Annual Review of Materials Science, 1976, 6, p. 139.
14. V. F. Zackay and E. R. Parker: Alloy Design, J. K. Tien and G. S. Ansell, eds., Academic Press, 1974.
15. B. V. N. Rao and G. Thomas: Intern. Journal of Frac., 1977, 13, 705.
16. R. W. K. Honeycombe: "Structure and Strength of Alloy Steels," Climax Moly. Co., London, 1975.

17. A. J. McEvily, R. G. Davies, C. L. Magee and T. L. Johnston: Symposium: Transformation and Hardenability in Steels, Climax Moly. Co., 1967, Ann Harbor, p. 179.

18. R. V. Fostini and F. J. Shoen: Symposium: "Transformation and Hardenability in Steels," Climax Moly. Co., 1967, Ann Harbor, p. 195.

19. M. G. Gemmil: Symposium on "Steel Strengthening Mechanisms," Climax Moly. Co., Zürich, 1969, p. 67.

20. A. P. Coldren, R. L. Cryderman and M. Semchyshen, Symposium on "Steel Strengthening Mechanisms," Climax Moly. Co., Zürich, 1969, p. 17.

21. B. V. N. Rao: Ph. D. Thesis, University of California, Berkeley, February 1978, LBL Report No. 7361.

22. J. R. Low, Jr., D. F. Stein, A. M. Turkalo, and R. P. Laforce: Trans. of AIME, 1968, 242, p. 14.

23 J. R. Rellick and C. J. McMahon, Jr.: Met. Trans., 1974, 5, p. 2439.

24. S. K. Banarji, C. J. McMahon, Jr., and H. C. Feng: Met. Trans. 1978, 9A, p. 237.

25. T. B. Cox and J. R. Low: Met. Trans., 1974, 5, p. 1457.

26. R. A. Grange: Met. Trans., 1971, 2, p. 65.

27. W. C. Leslie and G. C. Kauch: Met. Trans., 1978, 9A, p. 343.

28. G. R. Speich and W. C. Leslie: Met. Trans., 1972, 3, p. 1043.

29. G. Clark, R. O. Ritchie, and J. F. Knott: Nature Phys. Sci. (London), 1972, 239, p. 104.

30. G. Krauss and A. R. Marder: Met. Trans., 1971, 2, p. 2343.

31. T. Maki and C. M. Wayman: Acta. Met., 1977, 25, p. 681.

32. A. J. Baker, P. M. Kelly, and J. Nutting, "Phase Transformations," 1970, Metals Park, Ohio, ASM, p. 899.

33. R. M. Horn: Ph. D. Thesis, University of California, Berkeley, December 1976, LBL Report No. 5787.

34. M. S. Bhat: Ph. D. Thesis, University of California, Berkeley, February 1978, LBL Report No. 6046.

35. V. F. Zackay and E. R. Parker: "Fundamental Aspects of Structural Alloy Design," R. I. Jaffee and B. A. Wilcox, eds., Plenum Publ. Co., 1977, p. 109.

36. G. Thomas, I. Lin Cheng and J. R. Mihalisin: Trans. ASM, 1969, 62, p. 853.

37. S. K. Das and G. Thomas: Met. Trans., 1970, 1, p. 325.

38. O. Johari and G. Thomas: Acta. Met., 1965, 13, p. 1211.

39. Standart Method of Test for "Plain Strain Fracture Toughness of Metallic Materials," designation E 399-7, Annual ASTM Standardards, 1973, p. 960.

40. Yen-Lung Chem: Ph. D. Thesis, University of California, Berkeley, May 1976, LBL Report No. 5423.

41. M. F. Carlson, B. V. N. Bao, R. O. Ritchie and G. Thomas: Proc. Intern. Conf. on Strength of Metals and Alloys, Nancy, France, 1976, p. 509.

42. B. V. N. Rao, R. W. Miller and G. Thomas: Proc. 16th Intern. Heat Treatment Conf., The Metals Soc., London, 1976, p. 75.

43. M. Carlson: M. S. Thesis, University of California, Berkeley, June 1978, LBL Report No. 7670.

44. B. V. N. Rao, J. Y. Koo and G. Thomas: EMSA Proc., 1975, p. 30, Caliators Publ. Div., Baton Rouge.

45. A. K. Seal and R. W. K. Honeycombe, JISI, 1958, 188, p. 9.

46. Standard Methods for "Estimating the Average Grain Size of Metals," designation E 112.63, Annual ASTM Standards, 1973, p. 419.

47. B. Edmonson and T. Ko: Acta Met., 1954, 2, p. 235.

48. R. F. Heheman, K. R. Kinsman and H. I. Aaronson: Met. Trans., 1972, 3, p. 1077.

49. K. J. Irvine, F. B. Pickering on J. Garstone: JISI, 1960, 196, p. 65.

50. P. M. Kelly and J. Nutting, JISI, 1961, 183, p. 199.

51. J. D. Bolton, E. R. Petty and G. B. Allen: Met. Trans., 1971, 2, p. 2912.

52. V. F. Zackay, E. R. Parker, J. W. Morris, Jr., and G. Thomas: Materials Science and Engineering, 1974, 16, p. 201.

53. G. Thomas: JOM, 1977, 29, p. 31.

54. R. O. Ritchie and R. M. Horn: Met. Trans., 1978, 9A, p. 331.

55. G. Thomas: Met. Trans., 1978, 9A, p. 439.

56. R. M. Horn and R. O. Ritchie: Met. Trans., 1978, 9A, p. 1039.

57. G. Thomas and B. V. Narasimha Rao: Intern. Conf. on "Martensitic Transformation," Kiev, USSR, 1977.

58. B. V. Narasimha Rao: Univ. of Calif., Berkeley, July 1978, LBL Report No. 8013.

59. B. V. Narasimha Rao and G. Thomas: Paper submitted to Met. Trans., April 1979.

60. B. V. Narasimha Rao, M. Sarikaya and G. Thomas: submitted to 37th EMSA Conf., San Antonio, 1979.

TABLE I

	Cr	Mo	C	Mn	Ni	P	S	Fe	M_S (°C)	M_F (°C)	A_S (°C)	A_F (°C)
Alloy I	3.11	0.50	0.26	1.98	0.01	0.007	0.011	Bal.	320	260	765	800
Alloy II	3.01	0.51	0.25	0.08	2.00	0.007	0.009	Bal.	340	260	780	820

XBL 7811-6084

TABLE II

VARIATION OF AVERAGE PREAUSTENITE GRAIN SIZE WITH HEAT TREATMENT PRACTICE

Alloy \ H.T.	I	II	III	C	
I	270	40	35	30	Grain Size (μm)
II	180	25	20	25	

XBL 795-6242

Table III.
Mechanical Properties of Single Treated Steels

Alloys*	H.T.(I)** Tempering Temperature (°C)	Hardness (Rc)	YS (ksi)	UTS (ksi)	% Elongation		K_{IC} (ksi-in.$^{1/2}$)	Charpy V-Notch Energy (ft-lb)
					Uniform	Total		
Alloy I	As Quenched	48.5	200.0	253.0	3.50	6.25	80141	28.70
	200	48.0	205.0	257.0	2.60	7.05	110653	34.5
	300	45.0	177.0	206.0	2.80	8.00	--	22.50
	400	42.0	170.0	200.-	2.70	8.10	--	22.00
	500	40.5	166.0	194.0	3.70	7.00	--	20.00
	600	35.0	126.0	144.5	4.50	14.6	--	50.25
Alloy II	As Quenched	49.5	197.0	255.0	3.25	8.10	77652	31.40
	200	47.5	198.5	248.0	3.20	8.90	100156	35.25
	300	44.0	173.0	206.0	2.4	9.39	--	28.50
	400	43.0	167.0	194.0	2.6	10.5	--	27.00
	500	40.0	160.0	187.0	3.1	12.2	--	35.5
	600	35.5	128.5	145.5	5.2	16.8	--	90.25

*See Table I.
**See Figure 3.

Table IV.
Mechanical Properties of Single and Double Treated Steels

Heat Treatment*	Alloy**	Tempering Temperature	Hardness Rc	Y.S. ksi	U.T.S. ksi	% Elongation		Charpy V-Notch Energy ft/lb	K_{IC} ksi-in.$^{1/2}$
						Uniform	Total		
H.T.(I)	I	A.Q.	48.5	200.0	253.0	3.50	6.25	28.7	80141
		200	48.0	205.0	257.0	3.60	7.05	34.5	110653
	II	A.Q.	49.5	197.0	255.0	3.25	8.10	31.4	77652
		200	47.5	198.5	248.0	3.20	8.90	35.3	100156
H.T.(II)	I	A.Q.	49.0	194.0	252.0	3.50	9.55	32.0	--
		200	48.0	191.5	250.0	4.50	11.60	38.0	115724
	II	A.Q.	48.6	195.5	252.8	3.50	10.05	33.5	--
		200	48.0	188.0	245.0	4.30	11.60	38.0	93492
H.T.(III)	I	A.Q.	47.0	201.0	259.0	3.00	8.90	35.3	--
		200	47.0	194.0	250.0	4.50	12.00	42.0	118195
	II	A.Q.	47.0	199.0	251.5	3.25	11.55	34.3	--
		200	47.0	195.0	250.0	4.50	11.80	40.0	94505
H.T.(C)	I	A.Q.	45.0	199.0	259.0	4.00	8.90	22.0	--
		200	--	-	-	--	-	--	--
	II	A.Q.	45.5	192.0	248.0	3.90	10.50	22.5	--
		200	--	-	-	--	-	--	--

*See Figure 3.

**See Table I.

FIGURE CAPTIONS

Fig. 1. Schematic showing the desired duplex microstructure consisting of lath martensite and thin films of retained austenite.

Fig. 2. Sketches of round tensile (a), fracture toughness (b), and impact toughness (c) specimens.

Fig. 3. Schematic illustration of heat-treatments employed in this research.

Fig. 4. Optical micrographs of as quenched steels: (a), (c), and (e) are for Mn-containing steel, (b), (d), and (f) are for Ni-containing steel. (a) and (b) are from H.T.(I), (c) and (d) from H.T.(II), and (e) and (f) from H.T.(III).

Fig. 5. Bright field (BF) micrographs showing highly dislocated lath martensitic structure with autotempered carbides in the as-quenched condition (after H.T.(I)); (a) Mn containing, and (b) Ni containing steels.

Fig. 6. BF (a) and dark field (DF) (b) micrographs showing the extent of autotempering in the single treated, as-quenched Ni-containing steel. DF was taken using a superimposed reflection from martensite, retained austenite, and carbides. Note that the carbides are ε-carbides.

Fig. 7. BF (a), DF (b), selected area diffraction (SAD), pattern (c), and corresponding indexed pattern showing the Widmenstatten cementites in 200°C tempered Mn steel. Micrographs (e) and (f) show the carbide precipitation at dislocation inherited from murtensitic transformation. Micrograph (f) weak beam dark field (WBDF), of $0\bar{1}1_M$.

Fig. 8. BF (a), and DF (b) of 300°C tempered Mn-containing alloy. Note extensive twin carbide precipitation.

Fig. 9. BF (a) and DF (b), of 300°C tempered Ni-containing steel showing extensive carbide precipitation on microstructural twins. Note that twins are on $[121]_{\alpha}$. Also note the presence of widmenstatten carbides in BF (a).

Fig. 10. BF (a) and DF (b) of 400°C tempered Ni-containing steel showing extensive amount of widmenstatten precipitation.

Fig. 11. BF's (a) and (c) and DF's (b) and (d), of 400°C tempered Mn and Ni-containing steels, respectively, revealing the spheroidization of cementite. Arrows show the carbides precipitated from retained austenite.

Fig. 12. BF (a) and DF's (b) and (c); from widmenstatten cementite and spheroidized cementite, respectively, of 400°C tempered Ni-containing steel. Note the fine precipitates in micrograph (b) ($(MoCr_2)$ C or M_7C_3-carbides).

Fig. 13. BF micrographs of 200 (a), 300 (b) and 400°C (c), tempered Ni-containing steel showing the morphological changes through the tempering regimes.

Fig. 14. BF (a) and DF (b) micrographs revealing the microstructure of Alloy II at 500°C tempered condition. Note that (A) indicates widmenstatten cementites; (B) cementites decomposed from retained austenite at the lath boundaries, and (C) spheroidized cementites.

Fig. 15. DF-composite micrograph of Mn-containing alloy in the as-quenched condition revealing the interlath, thin films of retained austenite (H.T.(I)).

Fig. 16. BF (a), DF of $00\bar{2}A$ (b) and DF of 020M (c) showing the contrast change from austenite to martensite. SAD pattern (d) and the corresponding indexed pattern (e) show two variants of martensite, viz., [100] and [111], and single variant of austenite, viz., [100]. All from Ni containing steel in the as quenched condition after H.T.(I).

Fig. 17. BF and corresponding SAD patterns from twin-related laths 1 through 5 in the central packet (B) (Alloy I).

Fig. 18. Decomposition of retained austenite into interlath cementite stringers (indicated by arrows) in 300°C tempered Mn containing alloy.

Fig. 19. BF (a) and DF (b) micrographs showing the cementites decomposed from retained austenite following 400°C tempering in Ni-containing steel.

Fig. 20. Interlath precipitation of cementites in 400°C tempered Alloy I. (a) BF, (b) DF and (c) carefully indexed SAD pattern.

Fig. 21. BF (a), DF (b) and indexed SAD pattern (c) from 200°C tempered Alloy II revealing retained austenite films (double heat treatment H.T.(II)).

Fig. 22. BF (a) and DF (b) micrographs showing the extent of retained austenite phase in Mn-containing alloy (following H.T.(II) in the 200°C tempered condition).

Fig. 23. DF-composite micrograph of high amount of retained austenite formed in Ni-containing steel after application of H.T.(III).

Fig. 24. ε-carbides in Ni-containing alloy following H.T.(III) (200°C condition). (a) BF, (b) DF of an α reflection, (c) DF of a carbide reflection, and (d) indexed SAD pattern

Fig. 35. Inclusion characterization in Mn-containing alloy (200°C condition after H.T.(III)). (a) and (c) show inclusions situated at the dimples. (b) and (d) are corresponding X-ray spectrums.

Fig. 36. Comparison of toughness to strength relations in the experimental alloys and equivalent commercial alloys. (a) CVN-impact energy vs tensile strength, and (b) plane strain fracture toughness (K_{IC}) vs tensile strength.

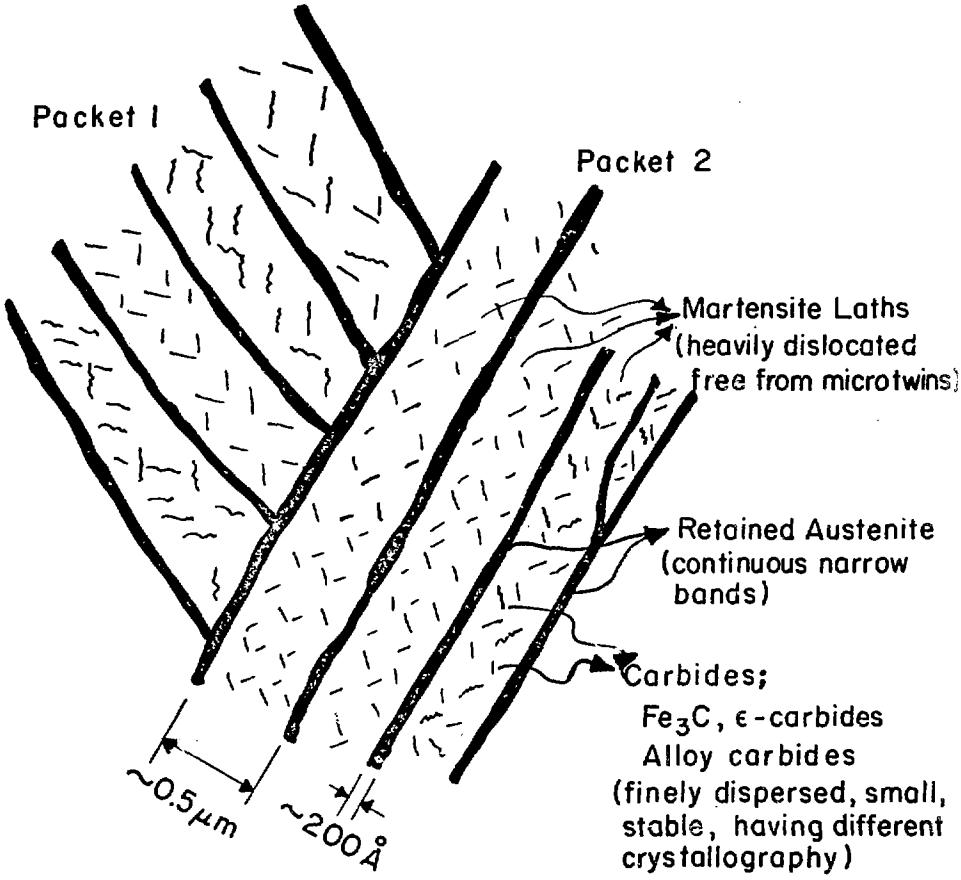
Packet 1
Packet 2
Martensite Laths
(heavily dislocated
free from microtwins)
Retained Austenite
(continuous narrow
bands)
Carbides;
Fe_3C, ε-carbides
Alloy carbides
(finely dispersed, small,
stable, having different
crystallography)
~0.5μm
~200Å
XBL794-6146

Fig. 1

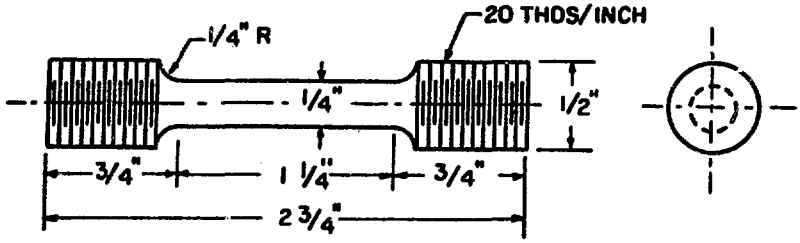

A. ROUND TENSILE SPECIMEN

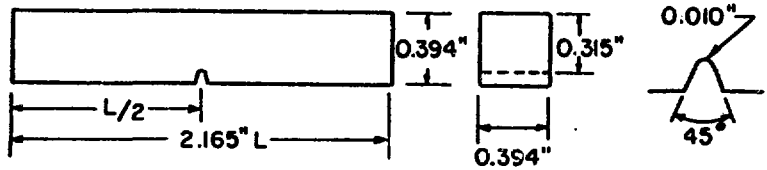

B. CHARPY V-NOTCH IMPACT SPECIMEN

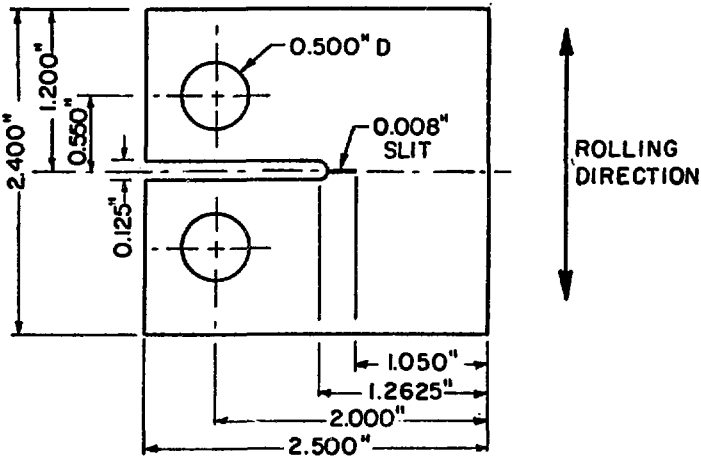

C. FRACTURE TOUGHNESS SPECIMEN

XBL 754-6176

Fig. 2

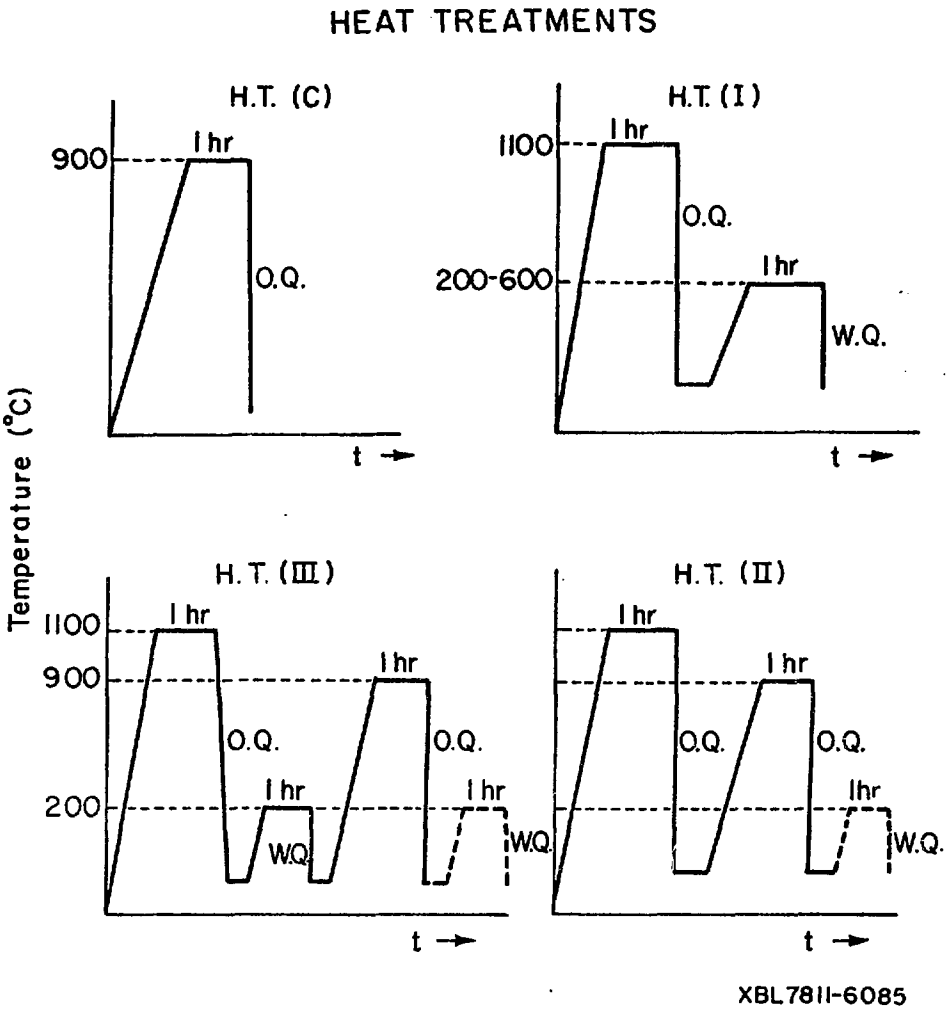
HEAT TREATMENTS
H.T. (C)
900
1 hr
O.Q.
t
H.T. (I)
1100
1 hr
O.Q.
200-600
1 hr
W.Q.
t
Temperature (°C)
H.T. (III)
1100
900
200
1 hr
O.Q.
1 hr
W.Q.
1 hr
O.Q.
1 hr
W.Q.
t
H.T. (II)
1 hr
O.Q.
1 hr
O.Q.
1 hr
W.Q.
t
XBL7811-6085

Fig. 3

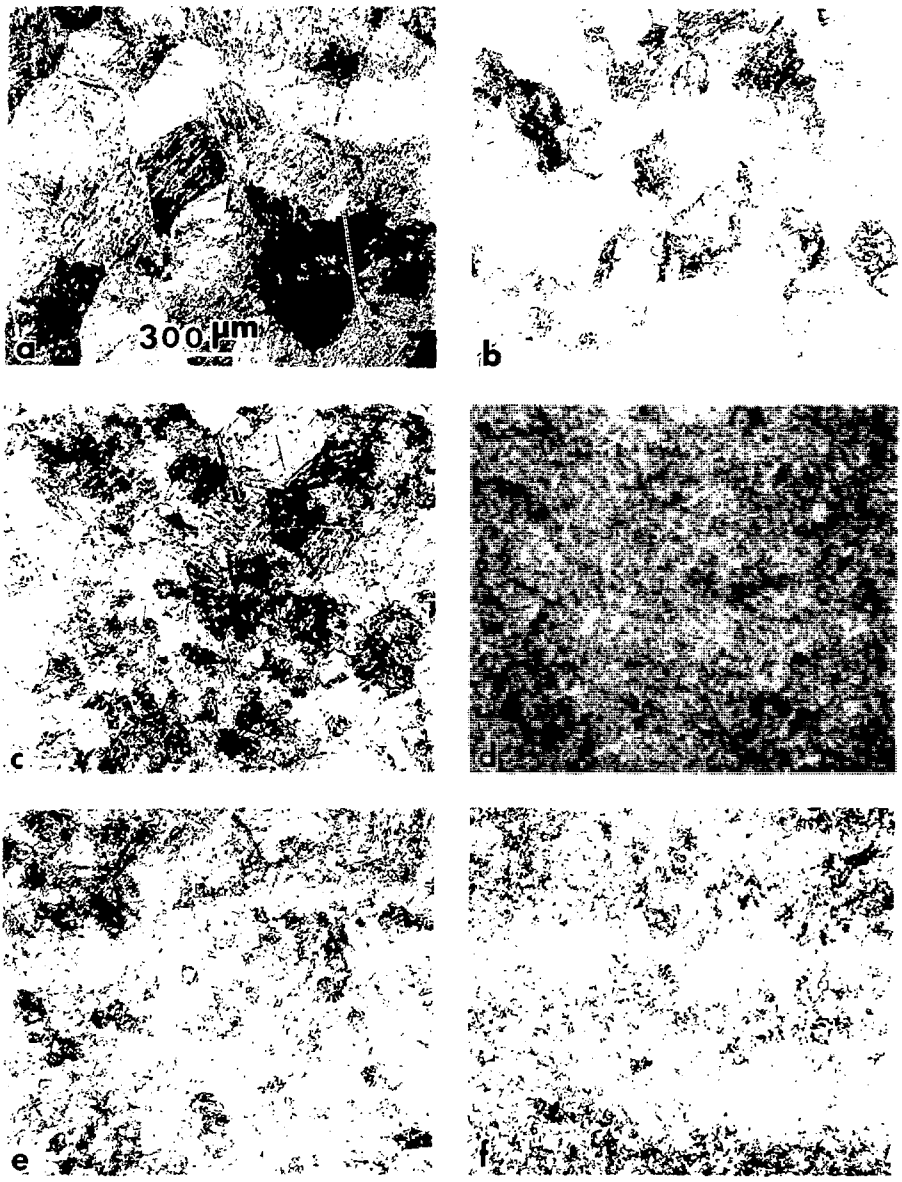

XBB 795-6493

Fig. 4

XBB 795-06494

Fig. 5

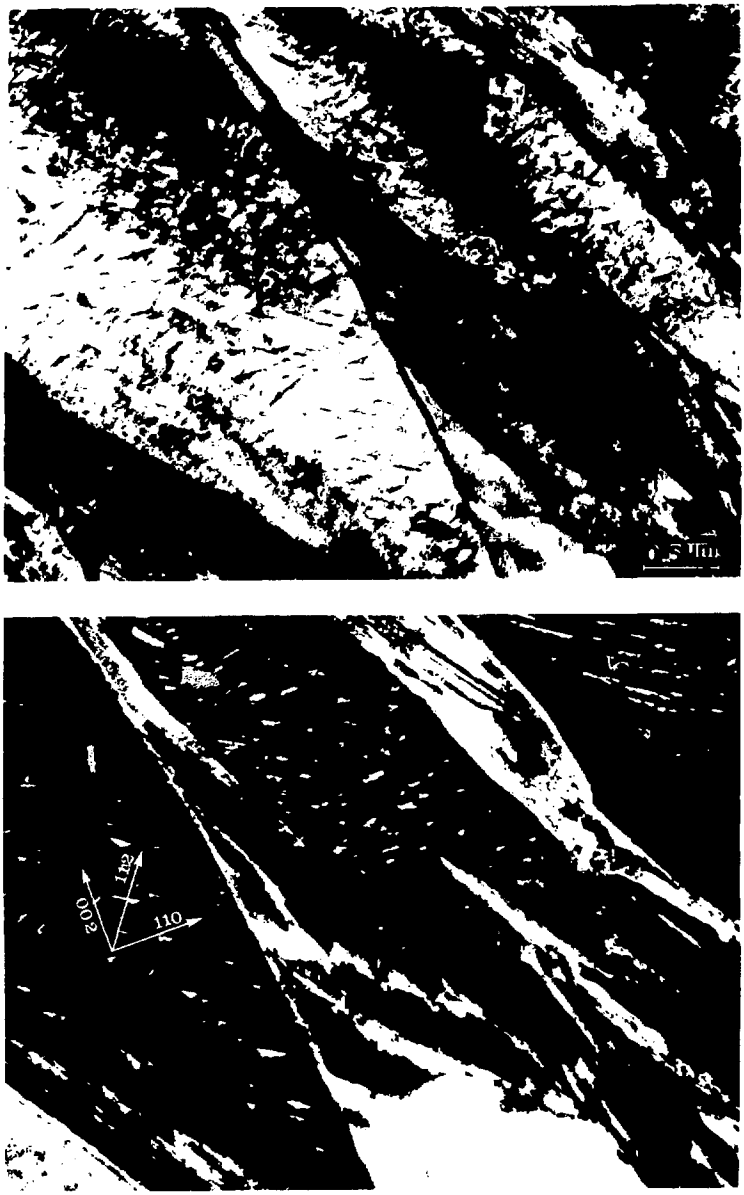

XBB 794-5475

Fig. 6

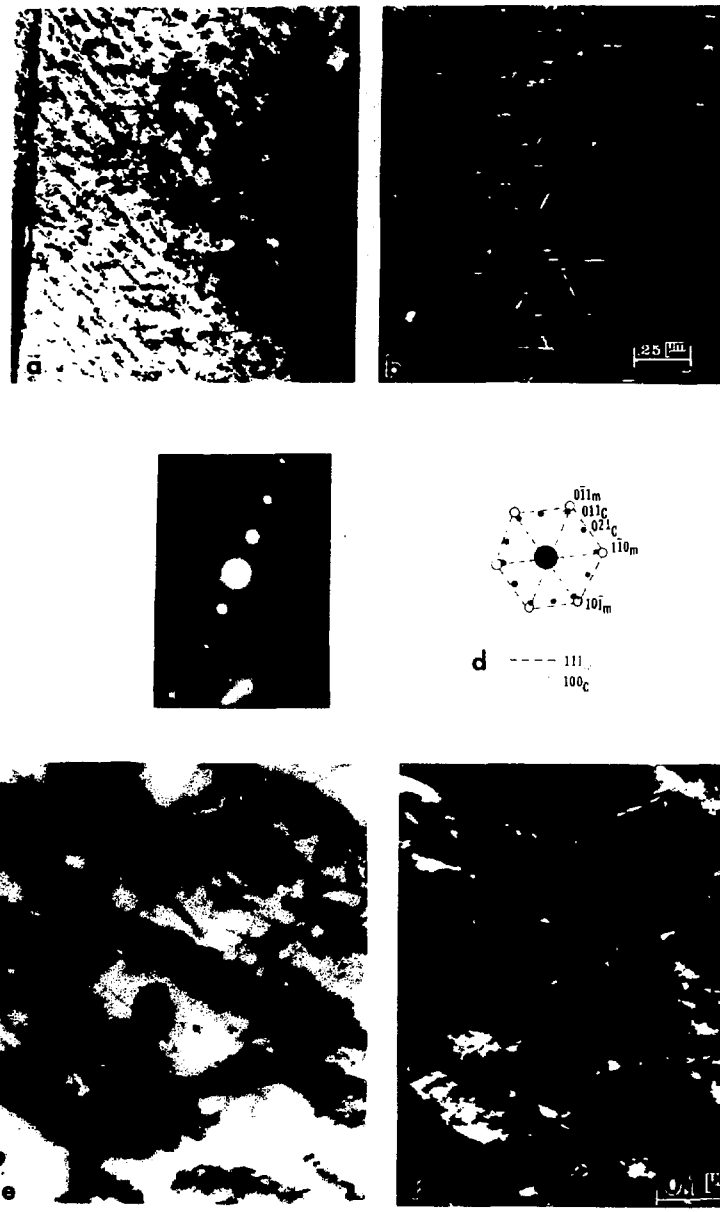

XBB 795-06263

Fig. 7

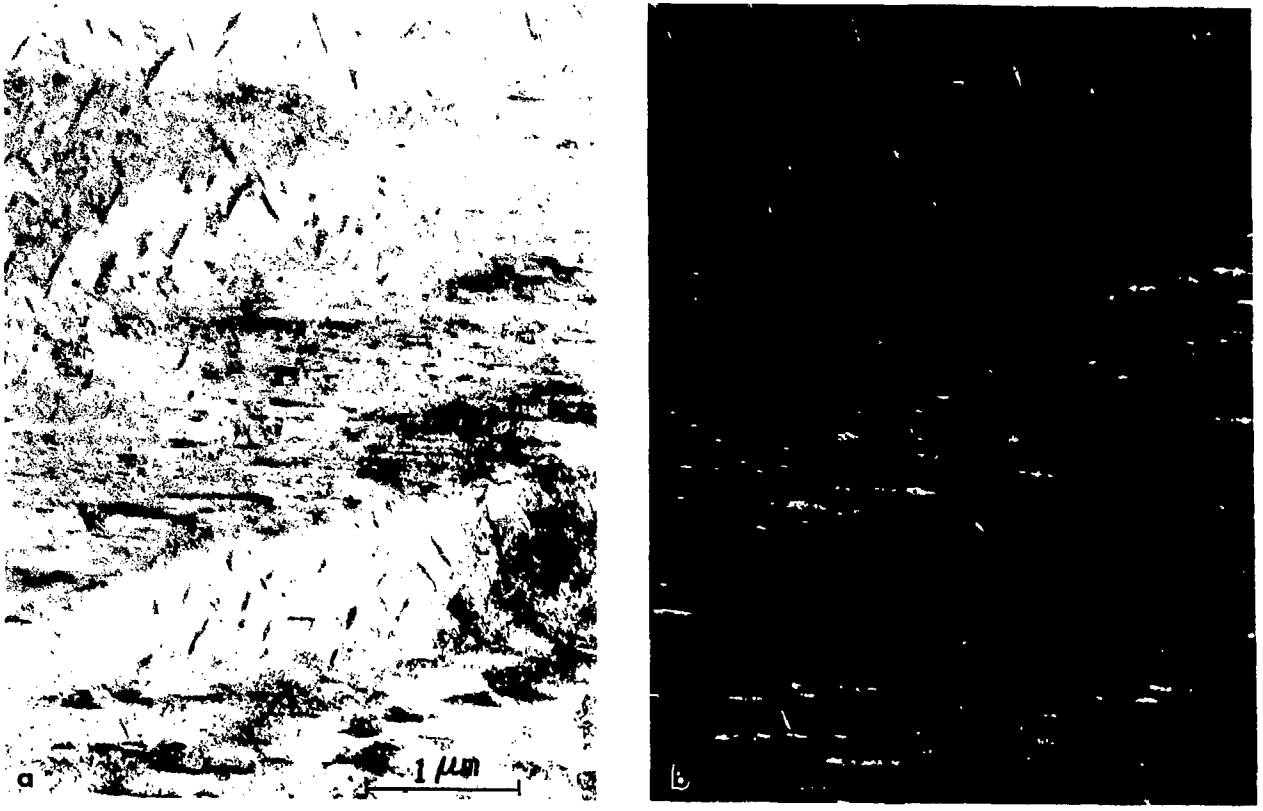

XBB 794-05672

Fig. 8

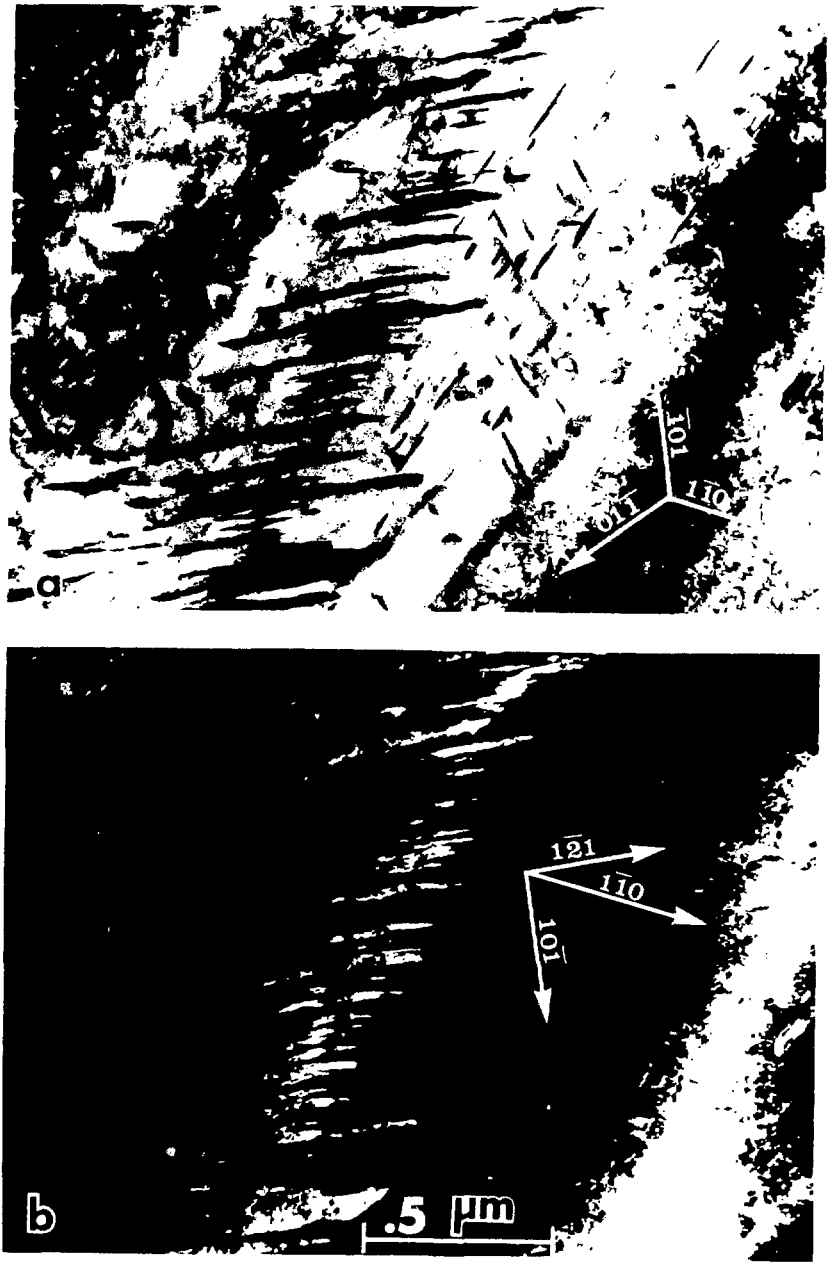

XBB 794-5823

Fig. 9

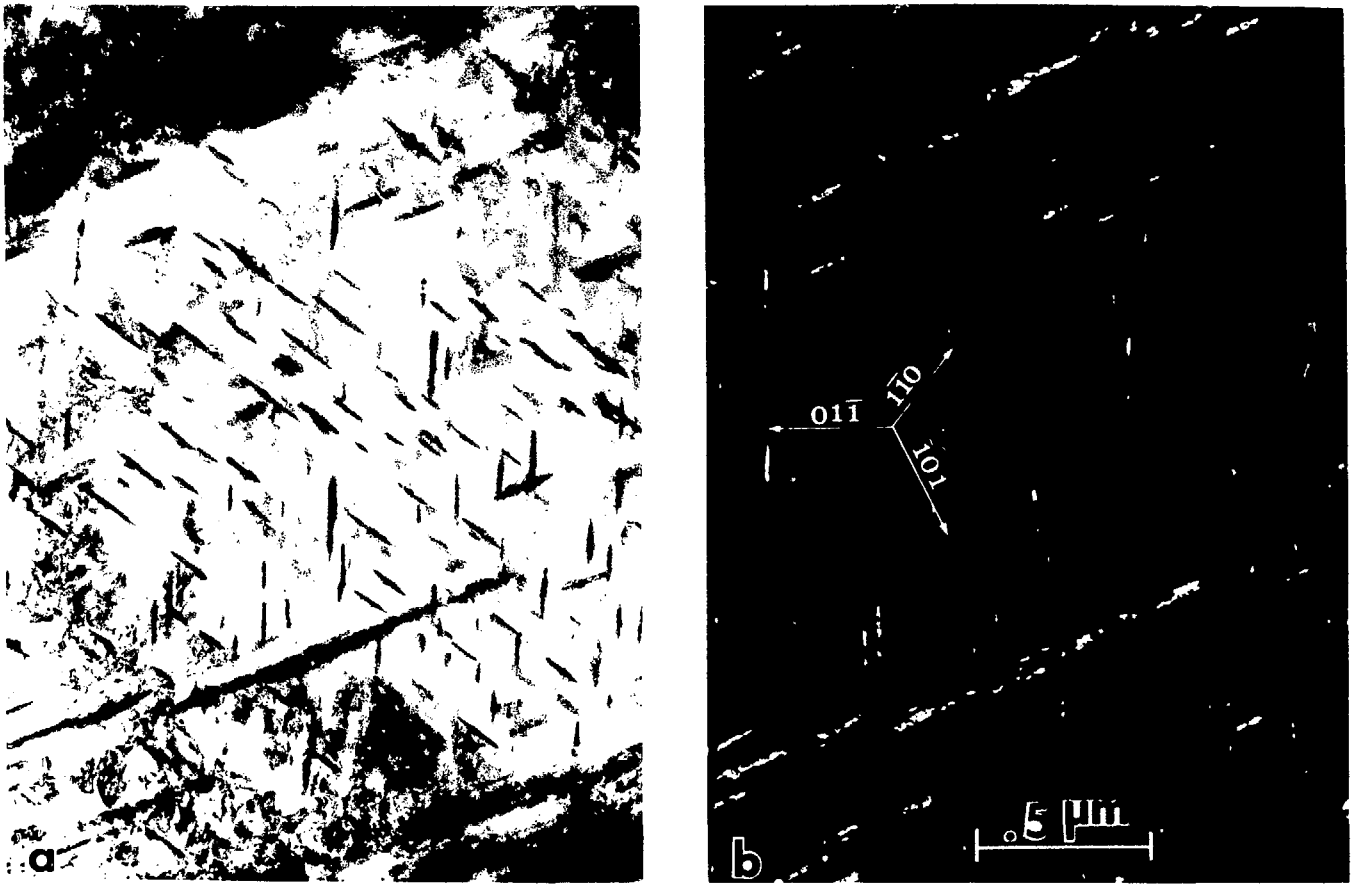

Fig. 10 XBB 794-05668

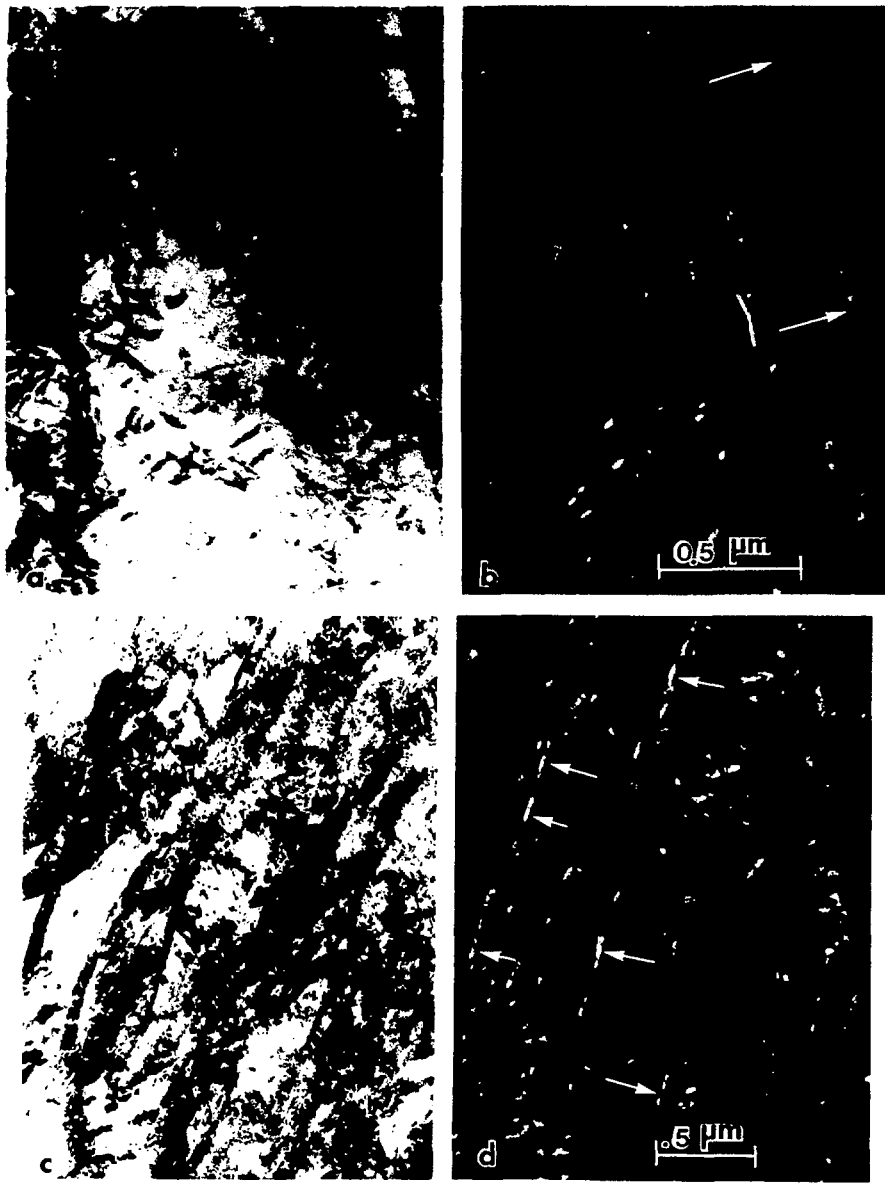

XBB 794-05661

Fig. 11

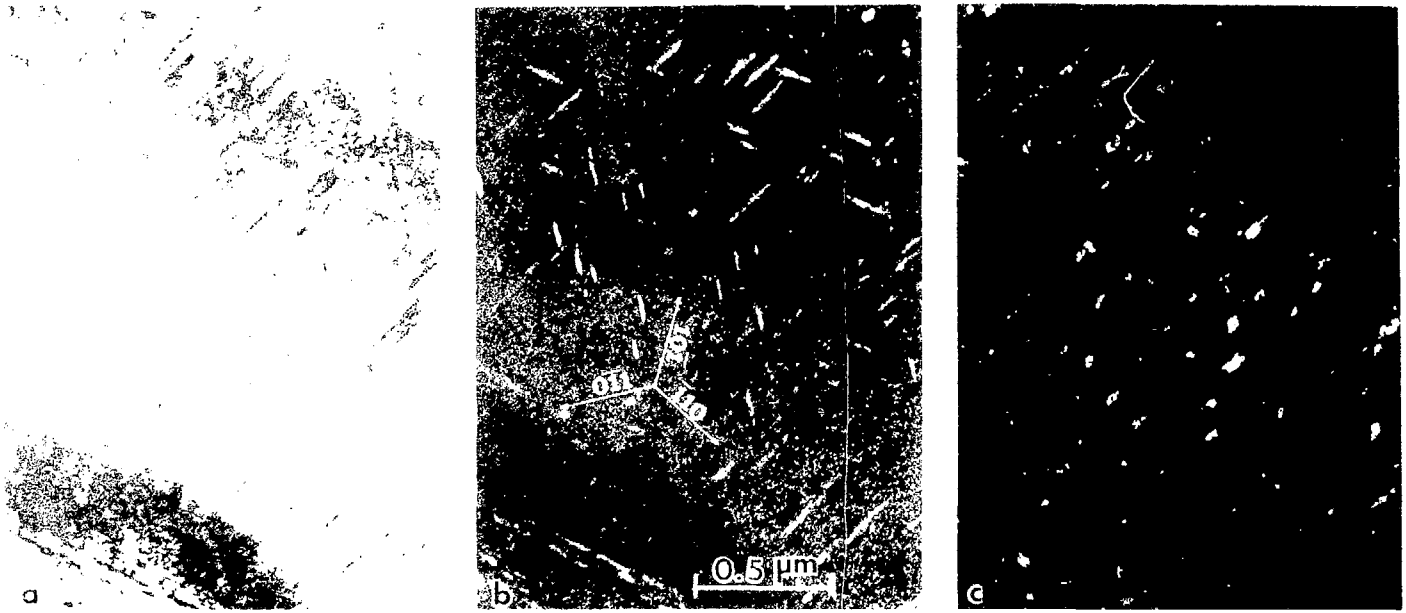

XBB 794-05679


a
1 µm

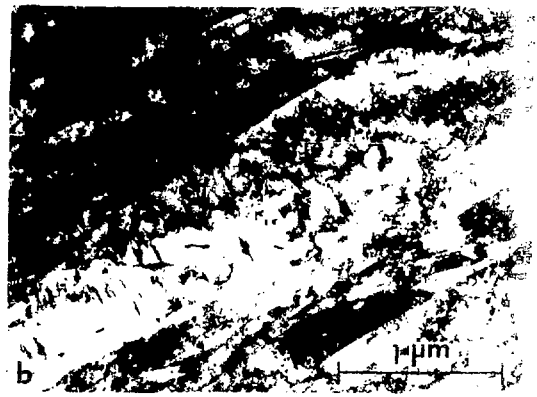
b
1 µm


c
1 µm

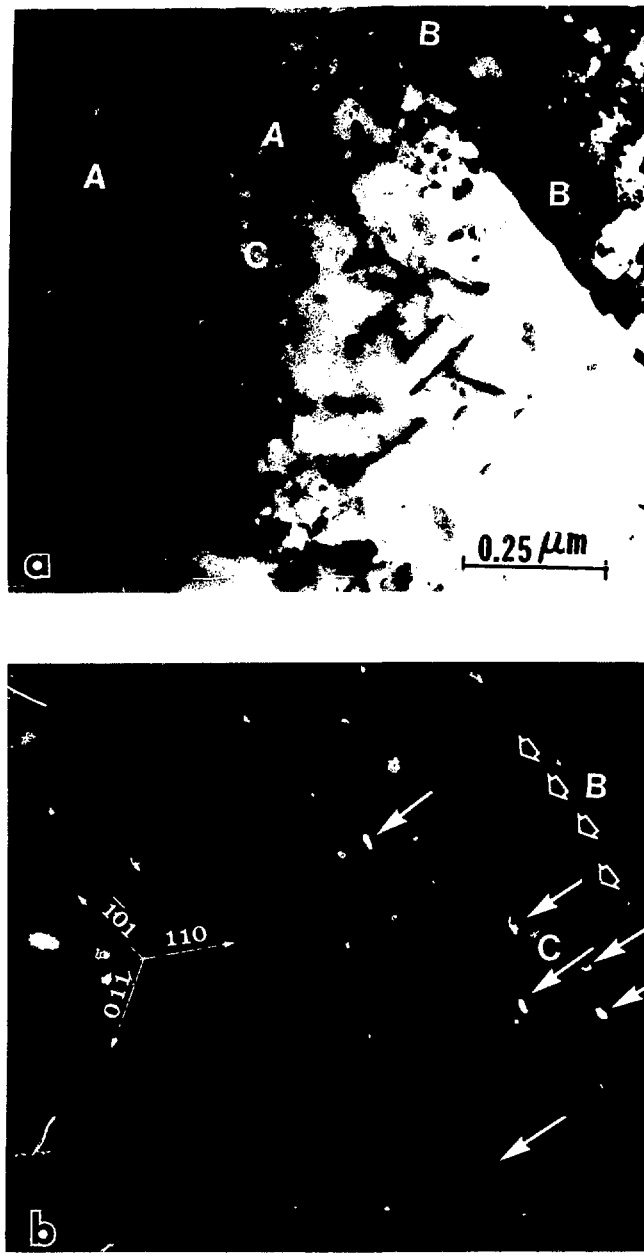

XBB 794-5871

Fig. 14

XBB 780-13949

Fig. 15

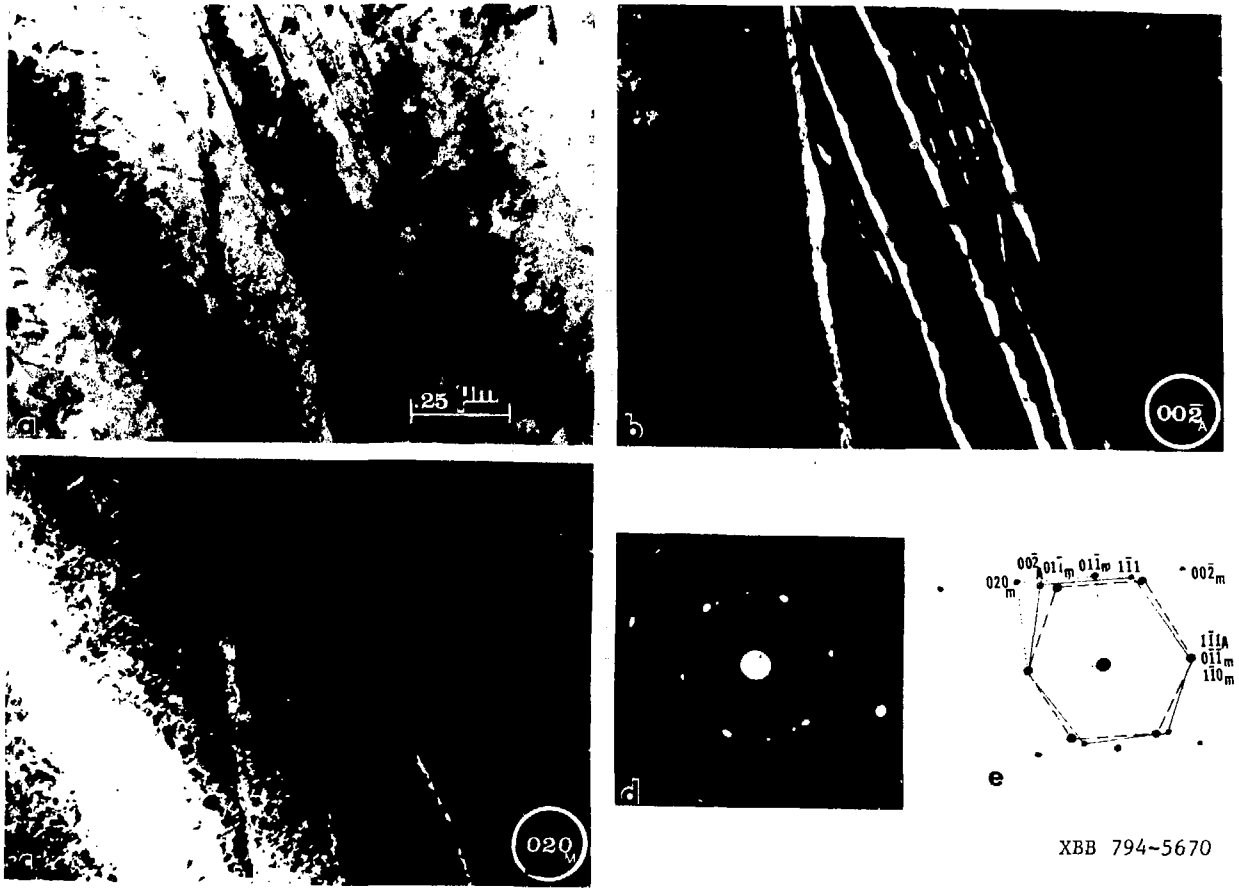
.25 μm
a
b
00$\bar{2}$
020
c
d
e
00$\bar{2}_A$
02$\bar{0}_m$
01$\bar{1}_m$
01$\bar{1}_m$
1$\bar{1}$
00$\bar{2}_m$
1$\bar{1}1_A$
01$\bar{1}_m$
1$\bar{1}0_m$
XBB 794-5670

Fig. 16

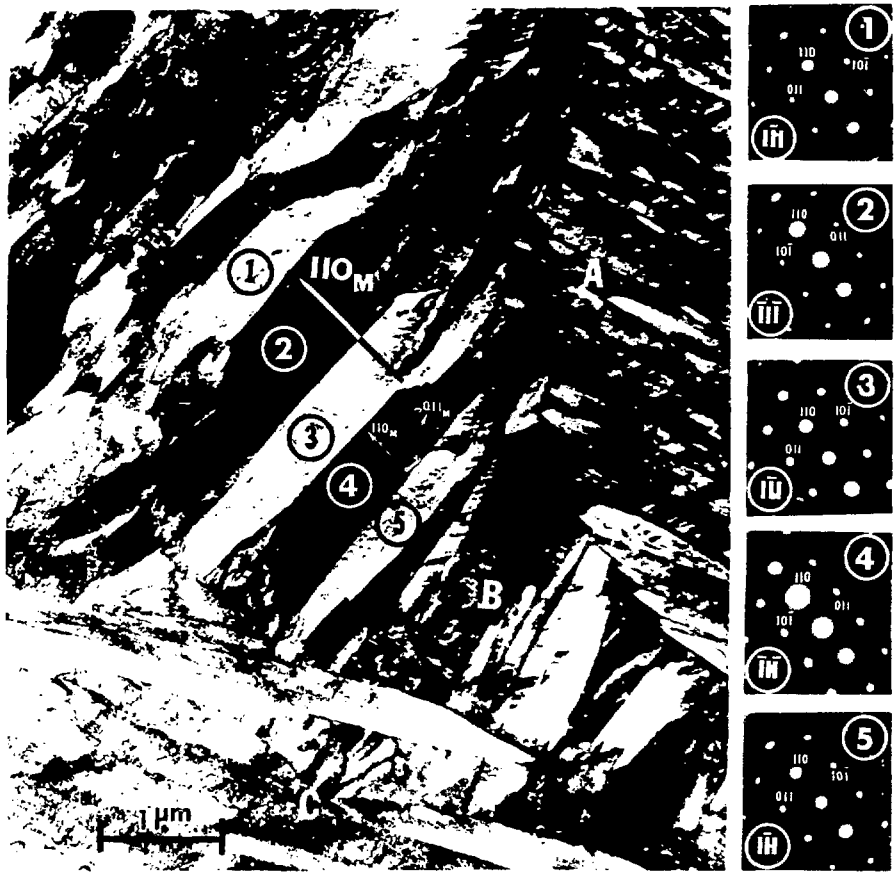

XBB 794-5820

Fig. 17

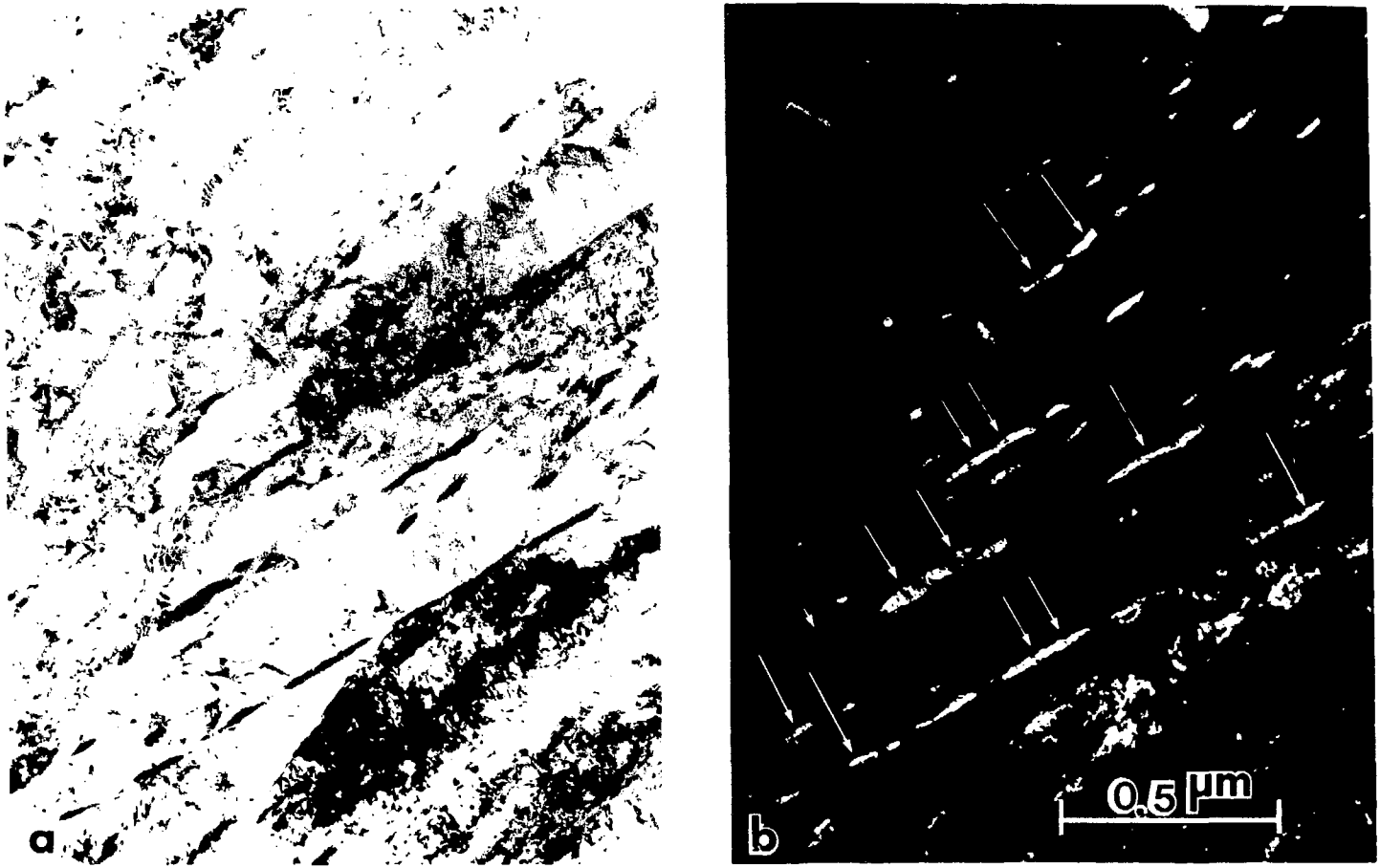

XBB 794-5669

Fig. 18

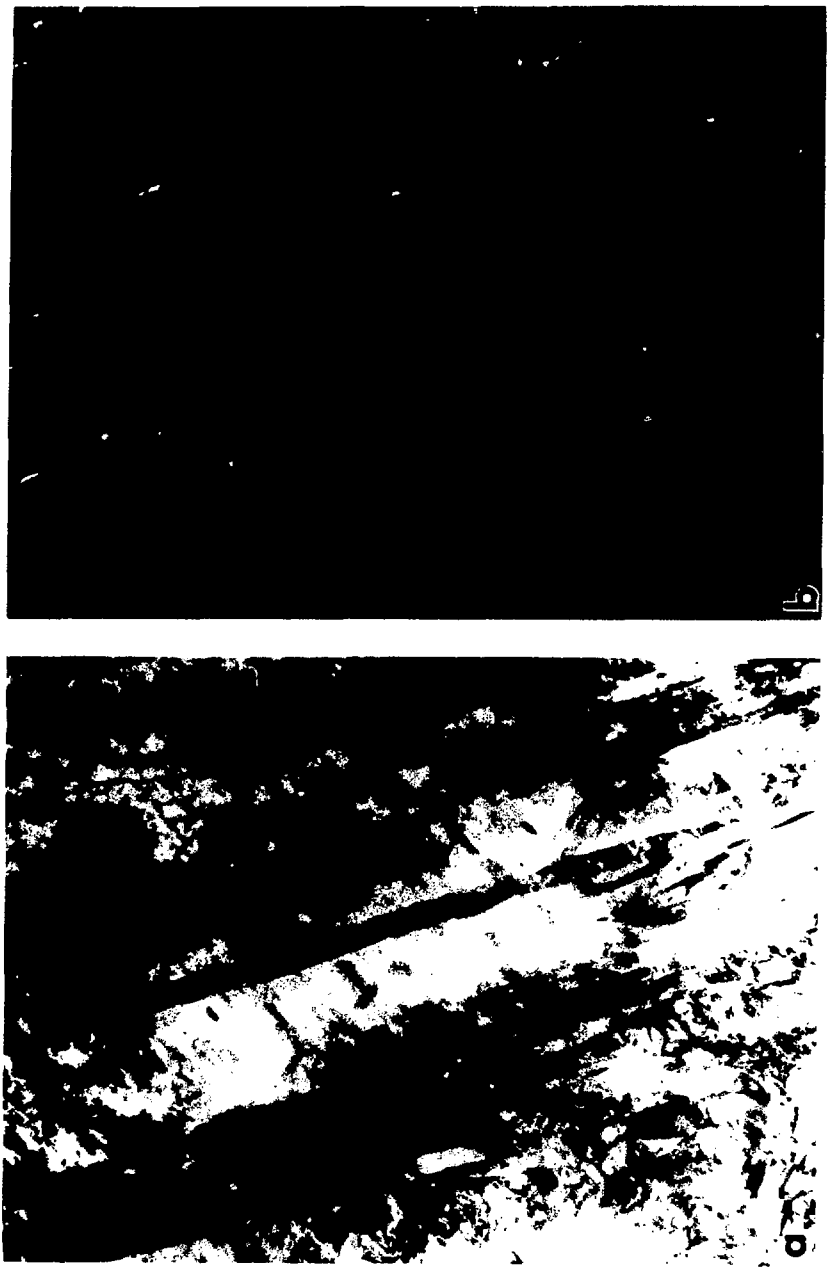

XBB 795-6424

Fig. 19

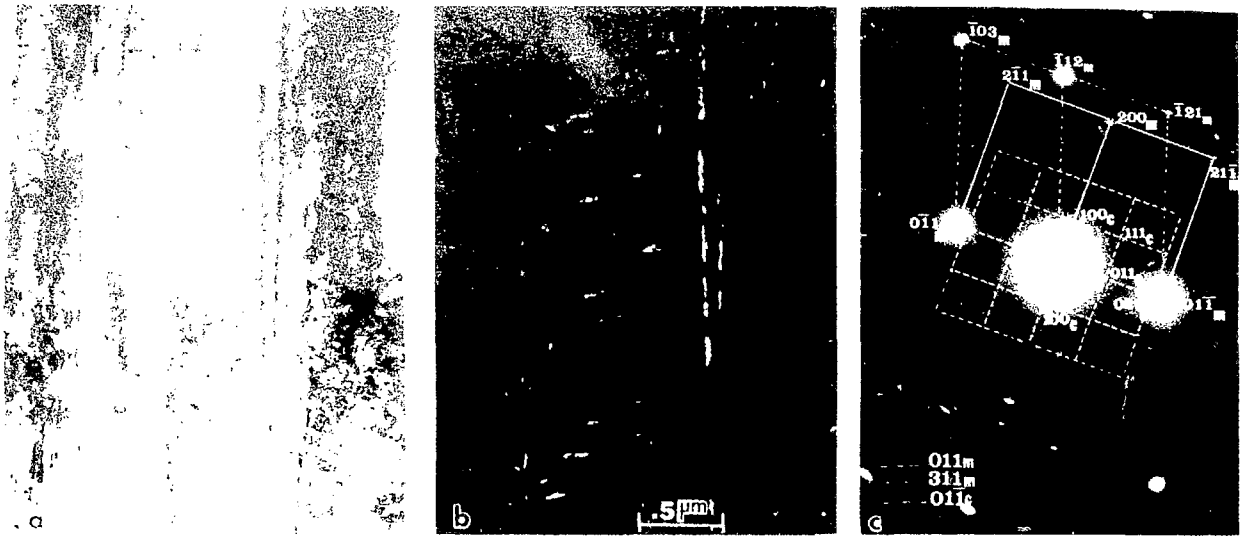
a
b
.5 μm
c
$\bar{1}03_m$
$\bar{1}12_m$
$2\bar{1}1_m$
200
$\bar{1}21_m$
$2\bar{1}\bar{1}_m$
$0\bar{1}1_m$
200_c
311_c
011_c
$\bar{1}\bar{1}1_m$
$\bar{2}00_c$
011_m
311_m
011_c

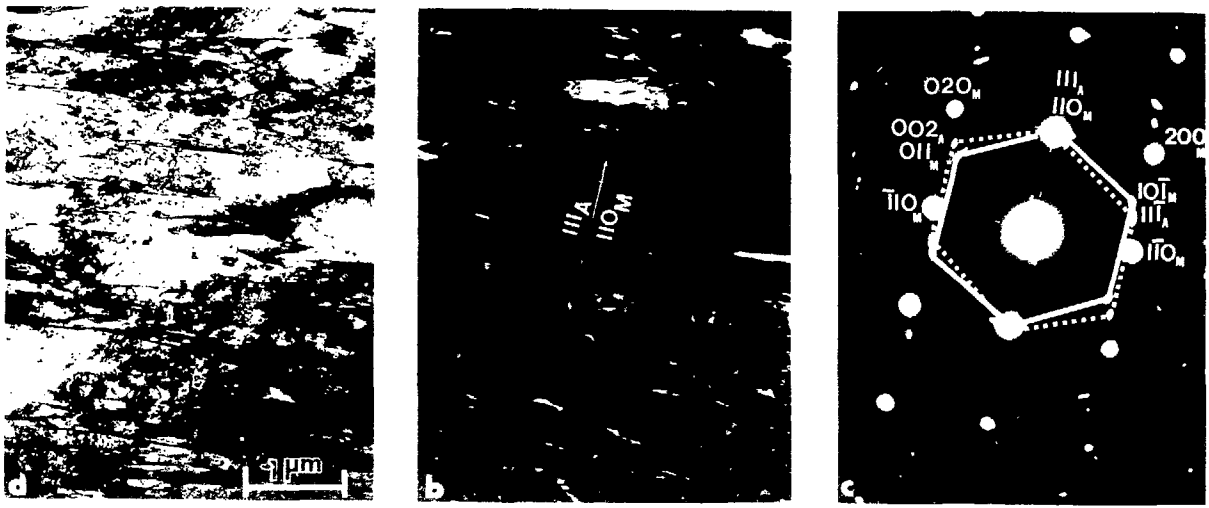
a
1 μm
b
111_A
110_M
c
020_M
111_A
110_M
002_A
011_M
200
$\bar{1}10_M$
$10\bar{1}_M$
111_A
$\bar{1}10_M$

XBB 794-4249

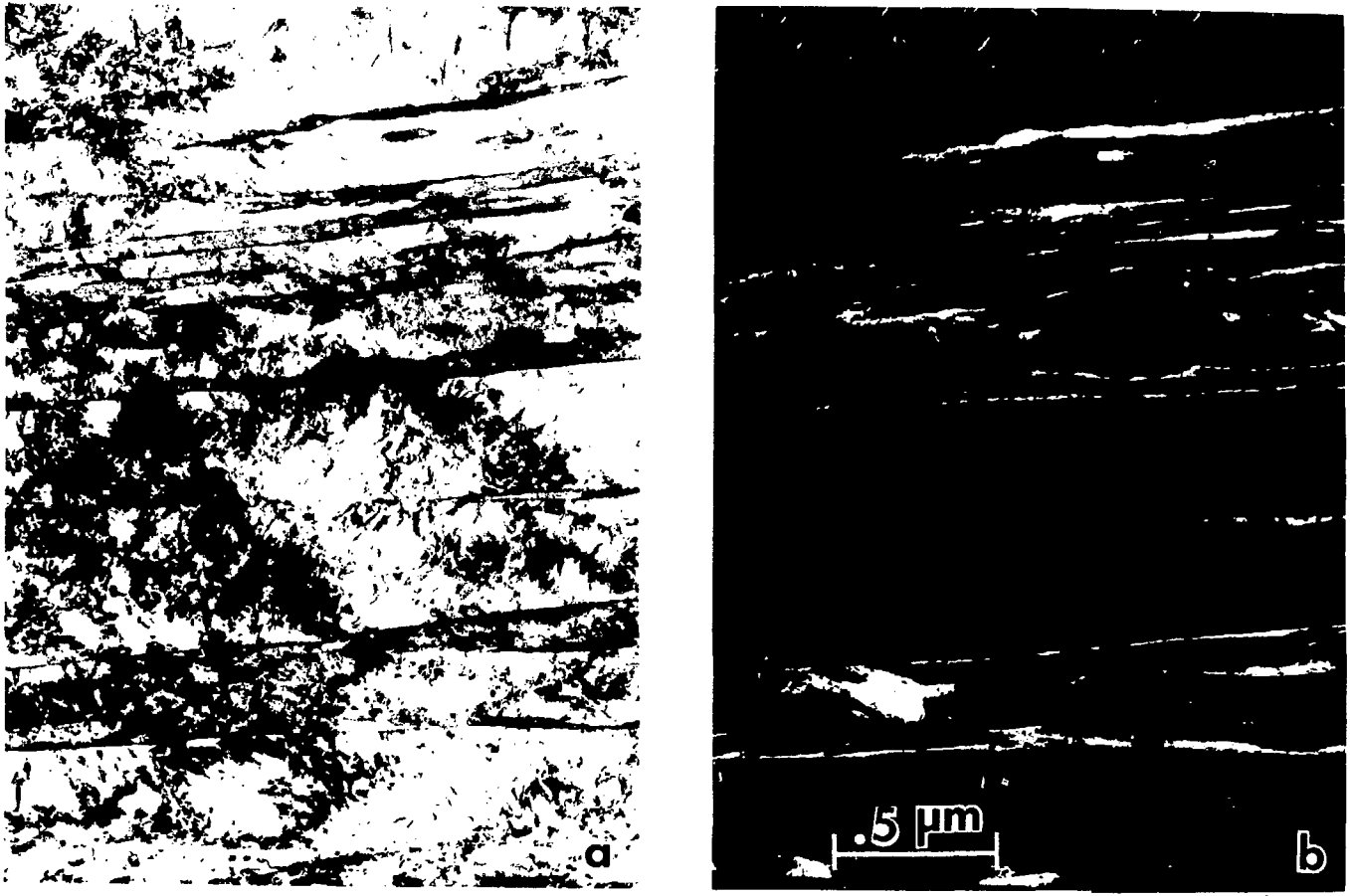

XBB 794-4551

Fig. 22

Fig. 23

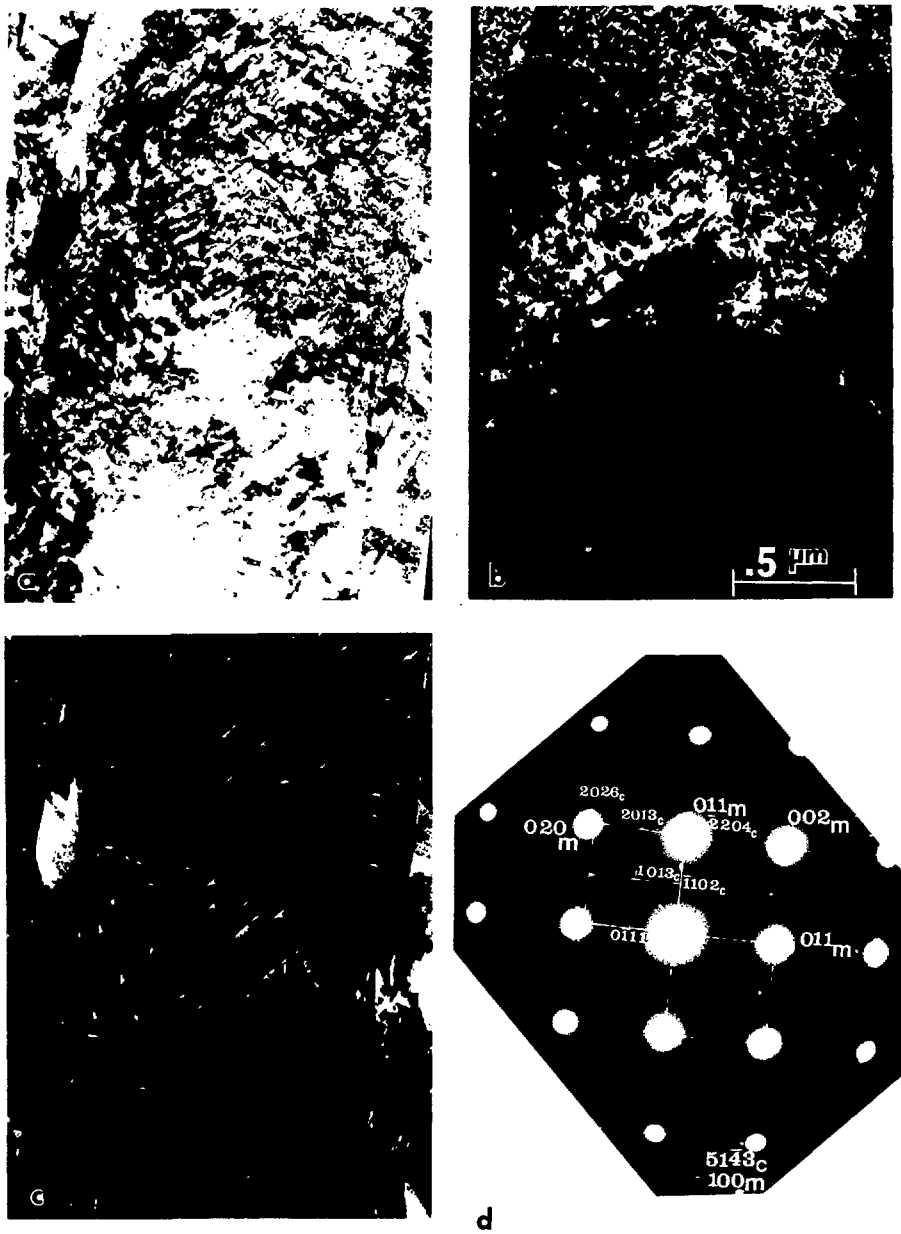

XBB 794-6924

Fig. 24

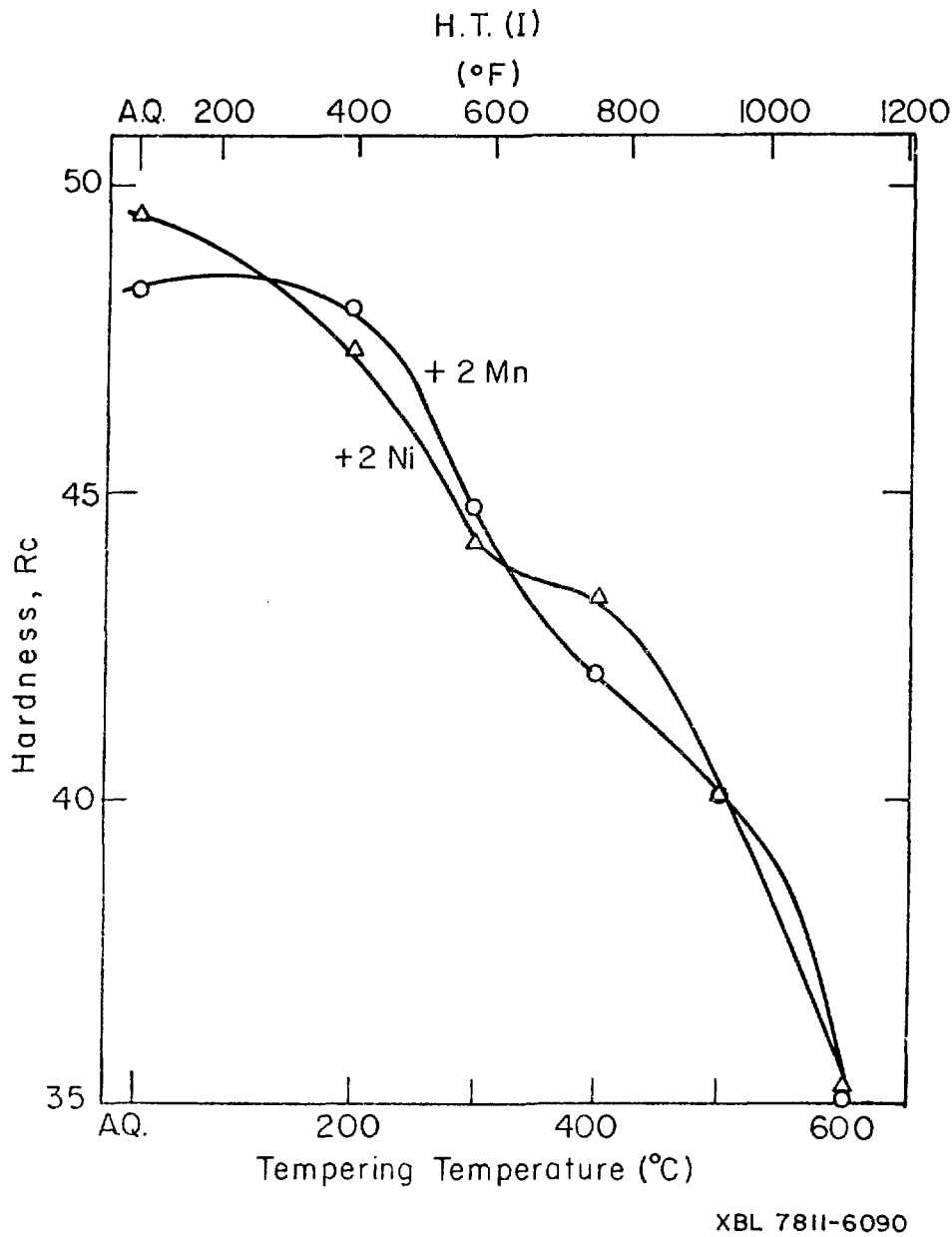
H.T. (I)
(°F)
A.Q.
200
400
600
800
1000
1200
50
45
40
35
Hardness, Rc
+ 2 Mn
+2 Ni
A.Q.
200
400
600
Tempering Temperature (°C)
XBL 7811-6090

Fig. 25

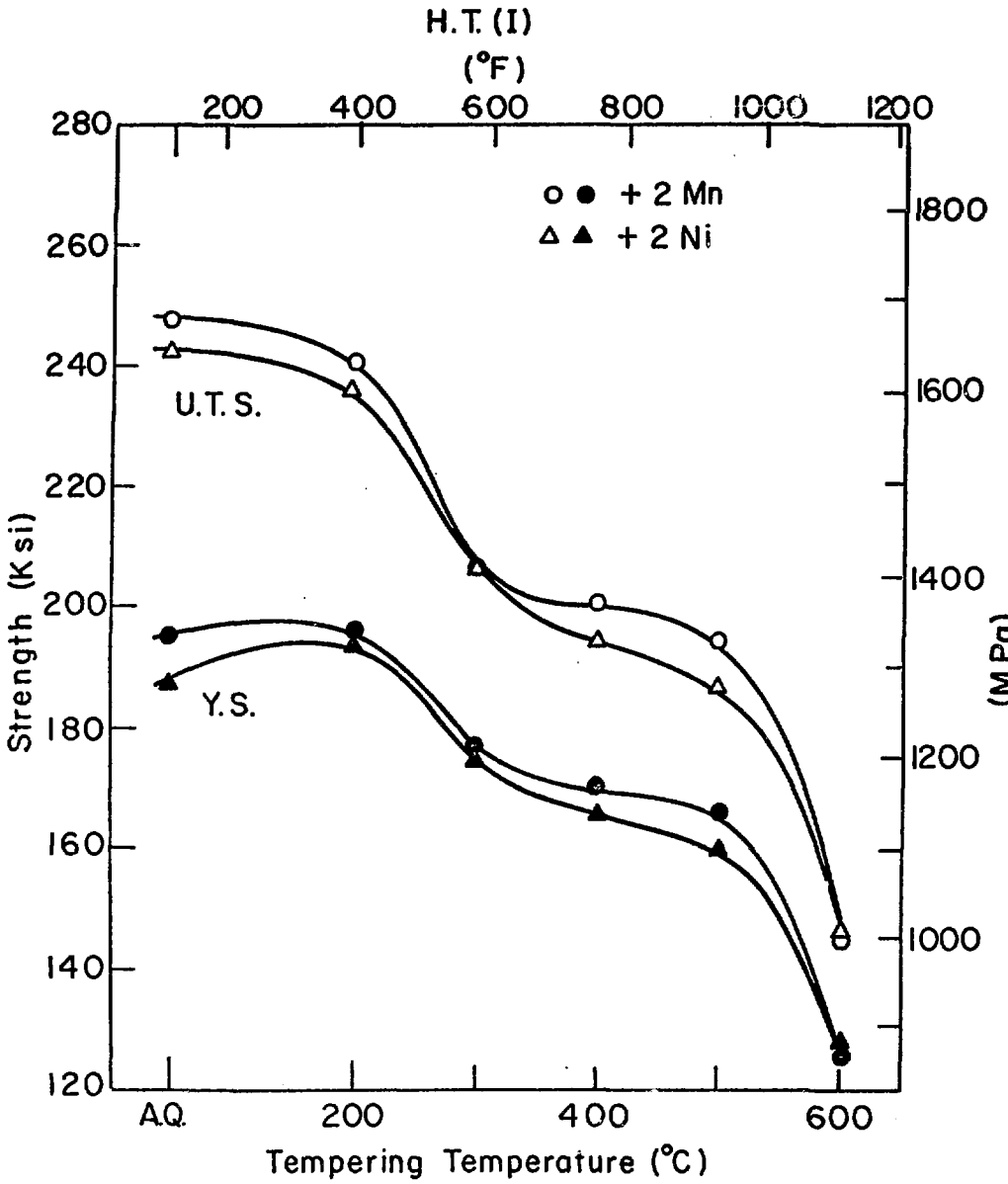
H.T. (I)
(°F)
200
400
600
800
1000
1200
280
260
240
220
200
180
160
140
120
o ● + 2 Mn
△ ▲ + 2 Ni
U.T.S.
Y.S.
Strength (Ksi)
1800
1600
1400
1200
1000
(MPa)
A.Q.
200
400
600
Tempering Temperature (°C)
XBL 7811-6091

Fig. 26

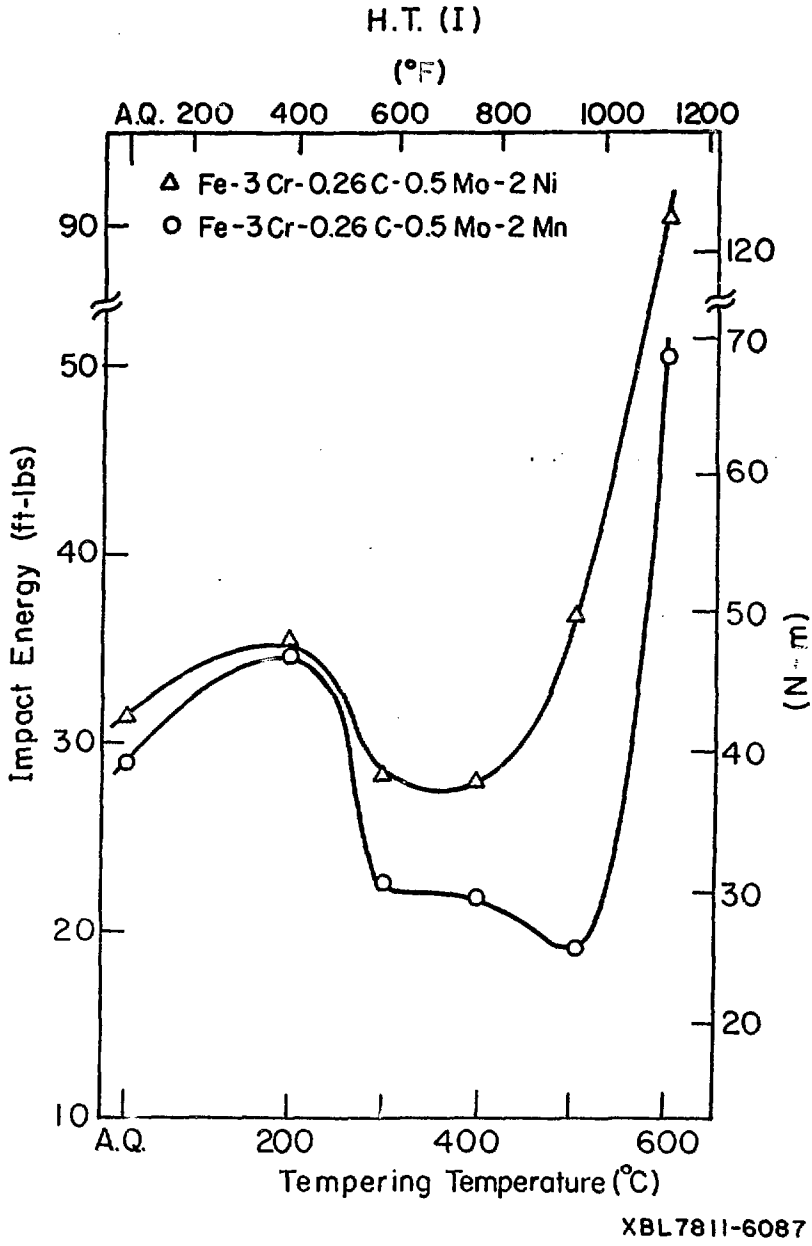
H.T. (I)
(°F)
A.Q. 200 400 600 800 1000 1200
Δ Fe-3Cr-0.26C-0.5Mo-2Ni
O Fe-3Cr-0.26C-0.5Mo-2Mn
Impact Energy (ft-lbs)
90
50
40
30
20
10
120
70
60
50
40
30
20
(N-m)
A.Q.
200
400
600
Tempering Temperature (°C)
XBL7811-6087

Fig. 27

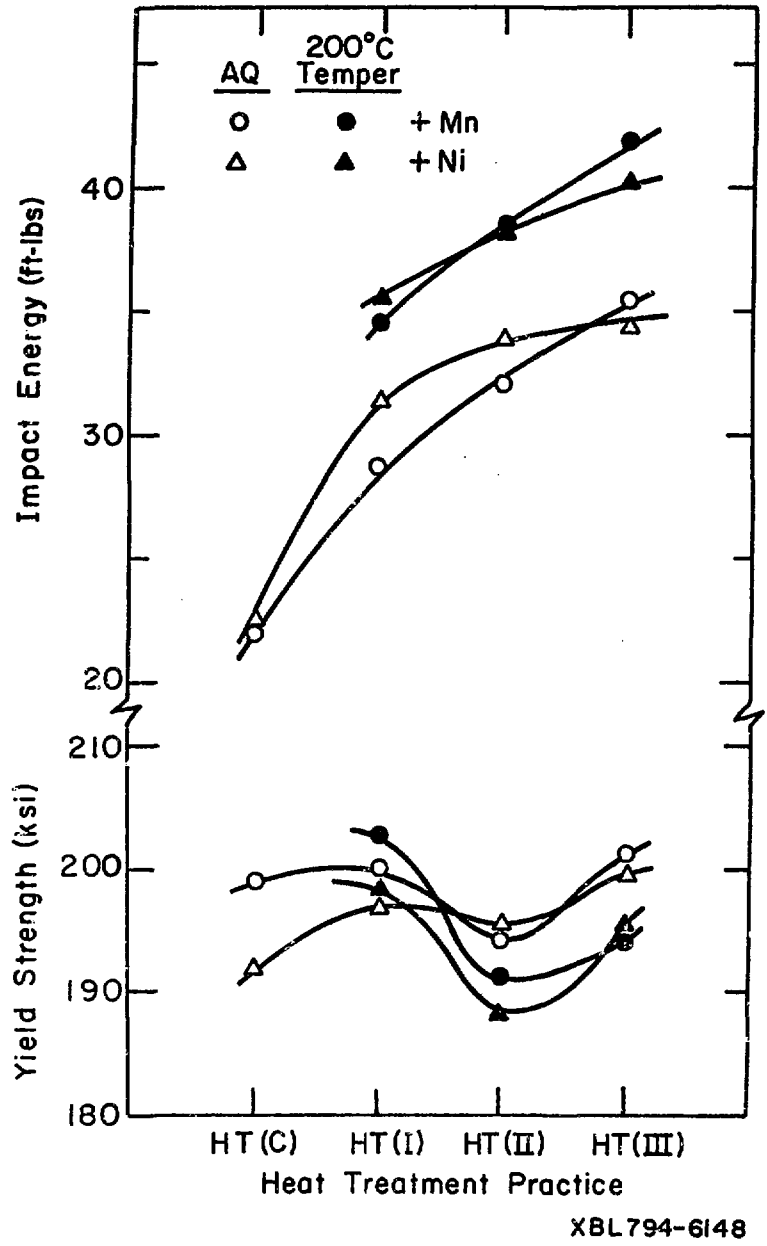
200°C
Temper
AQ
+ Mn
+ Ni
Impact Energy (ft-lbs)
40
30
20
Yield Strength (ksi)
210
200
190
180
HT(C)
HT(I)
HT(II)
HT(III)
Heat Treatment Practice
XBL794-6148

Fig. 28a

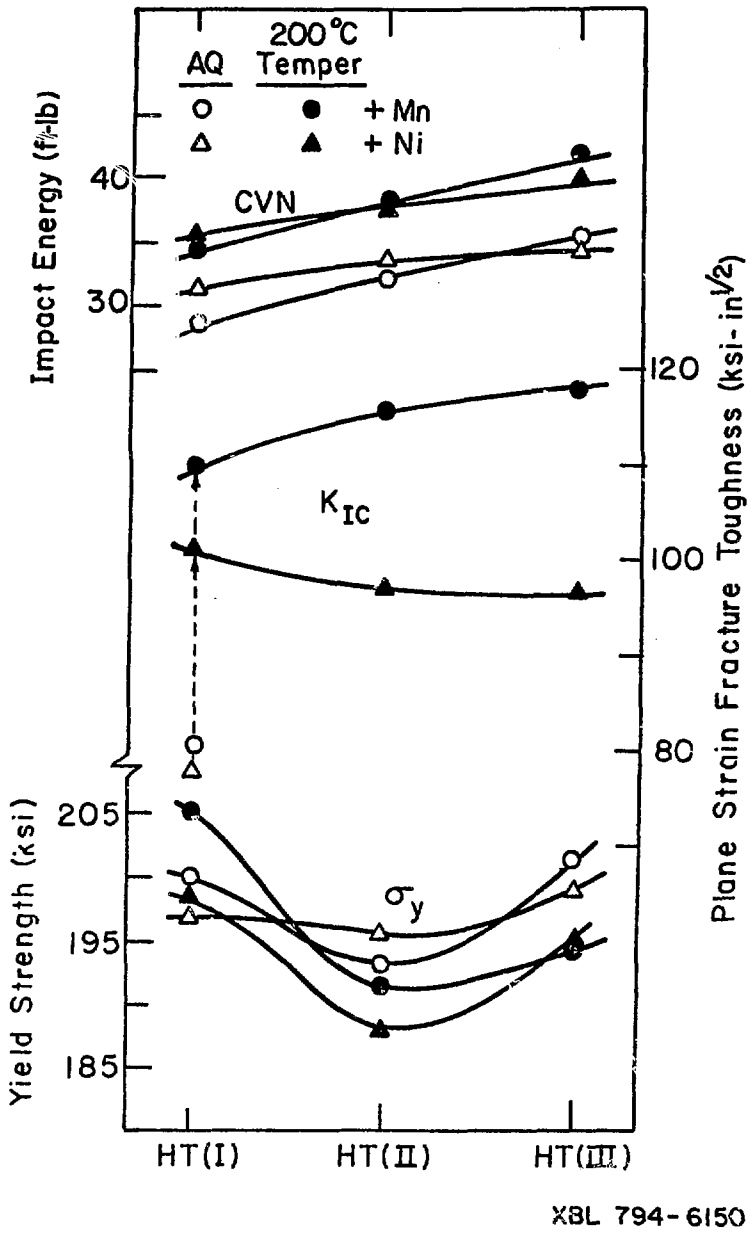
200°C
AQ Temper
+ Mn
+ Ni
CVN
K_{IC}
σ_y
Impact Energy (ft-lb)
Yield Strength (ksi)
Plane Strain Fracture Toughness (ksi-in$^{1/2}$)
40
30
205
195
185
120
100
80
HT(I)
HT(II)
HT(III)
XBL 794-6150

Fig. 28b

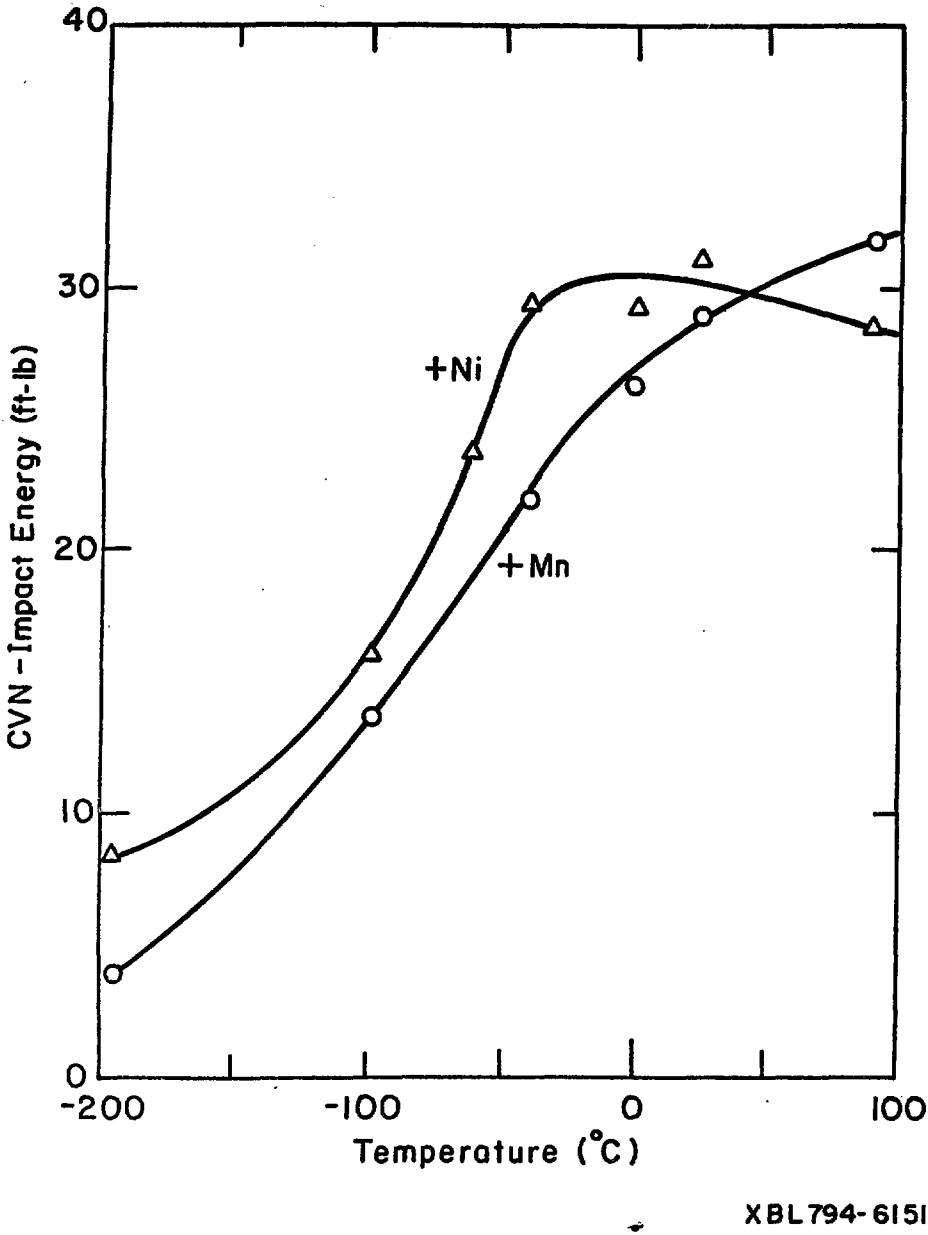
40
30
20
10
0
CVN - Impact Energy (ft-lb)
+Ni
+Mn
-200
-100
0
100
Temperature (°C)
XBL794-6151

Fig. 29

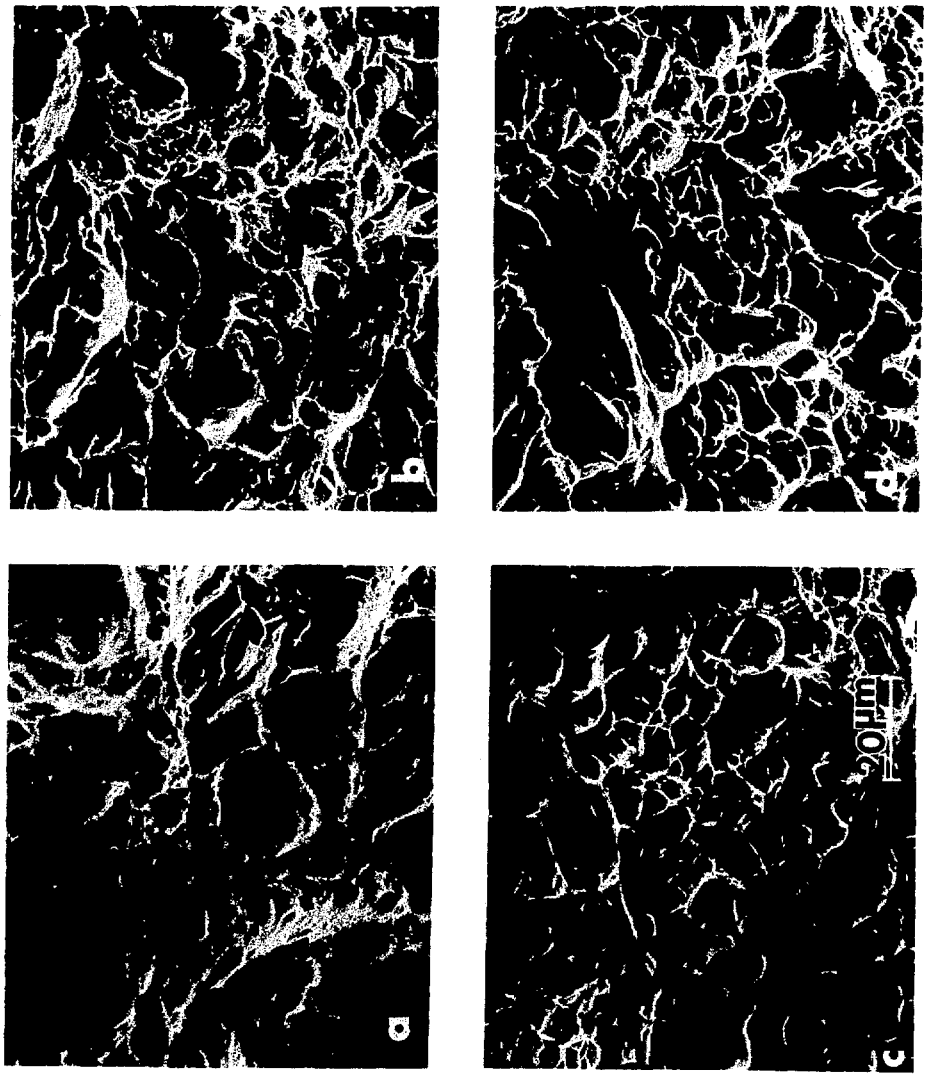

XBB 794-5471

Fig. 30

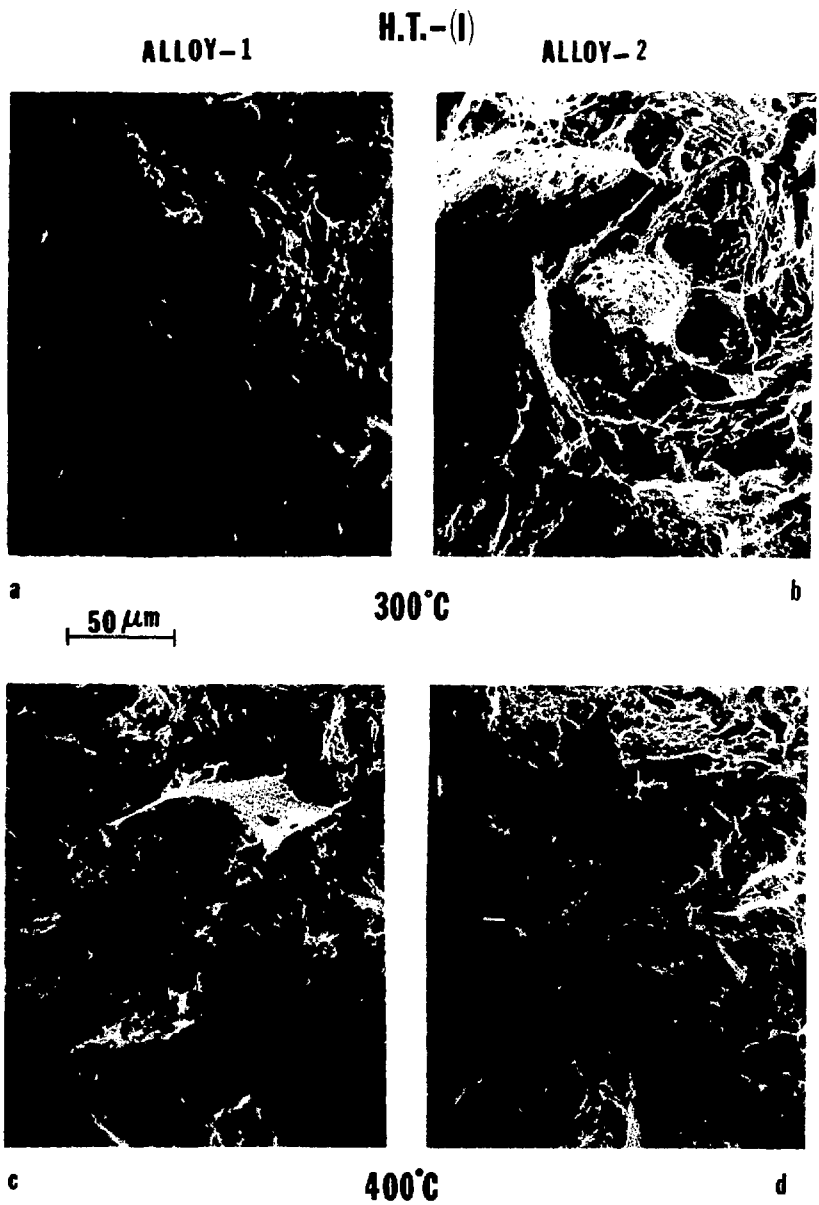

XBB 780-13909

Fig. 31

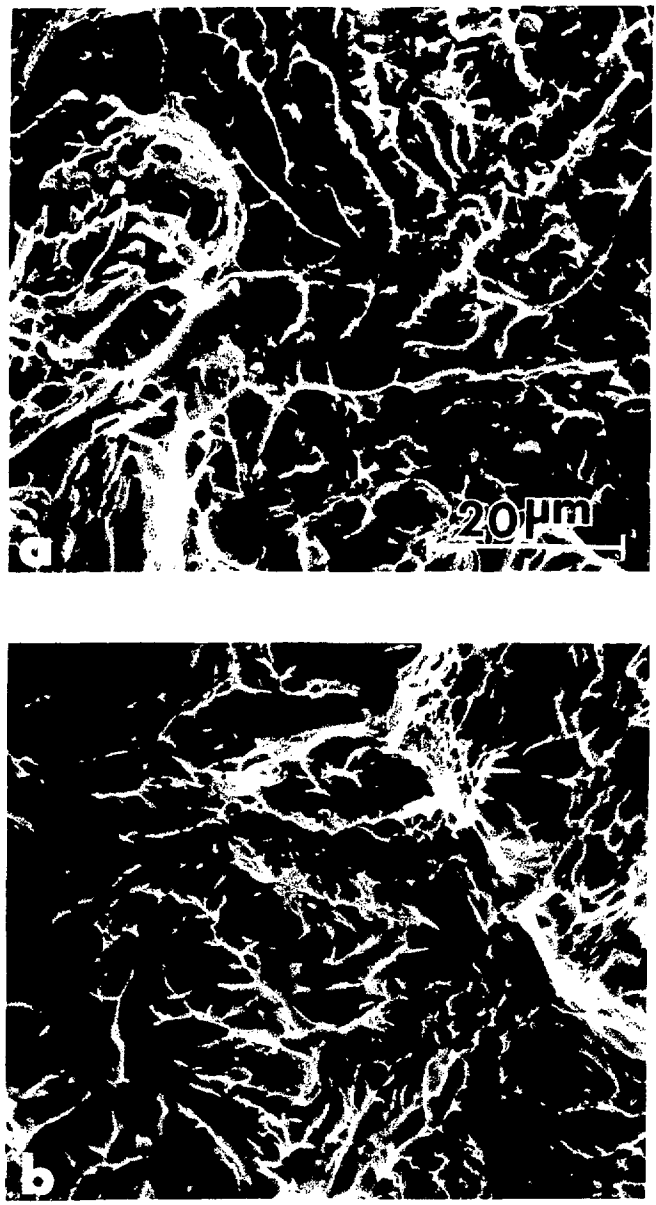

XBB 794-5470

Fig. 32

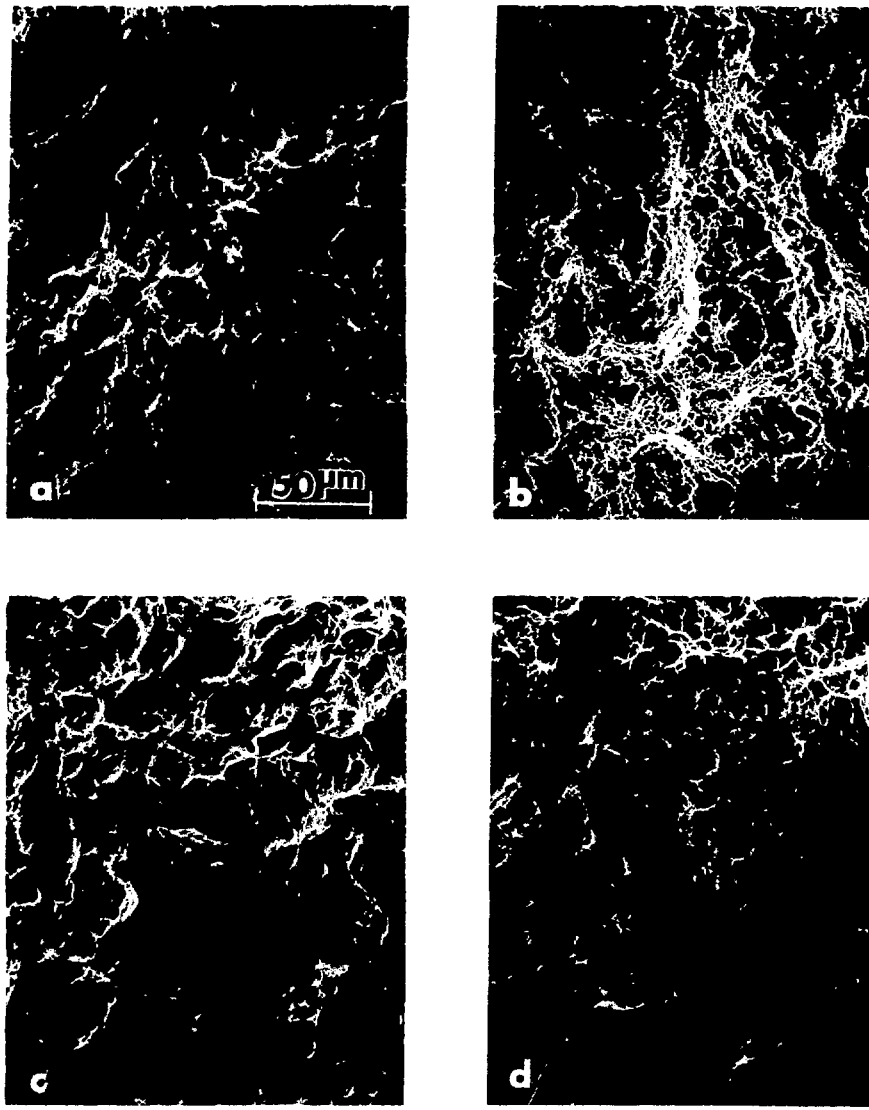

XBB 794-05472

Fig. 33

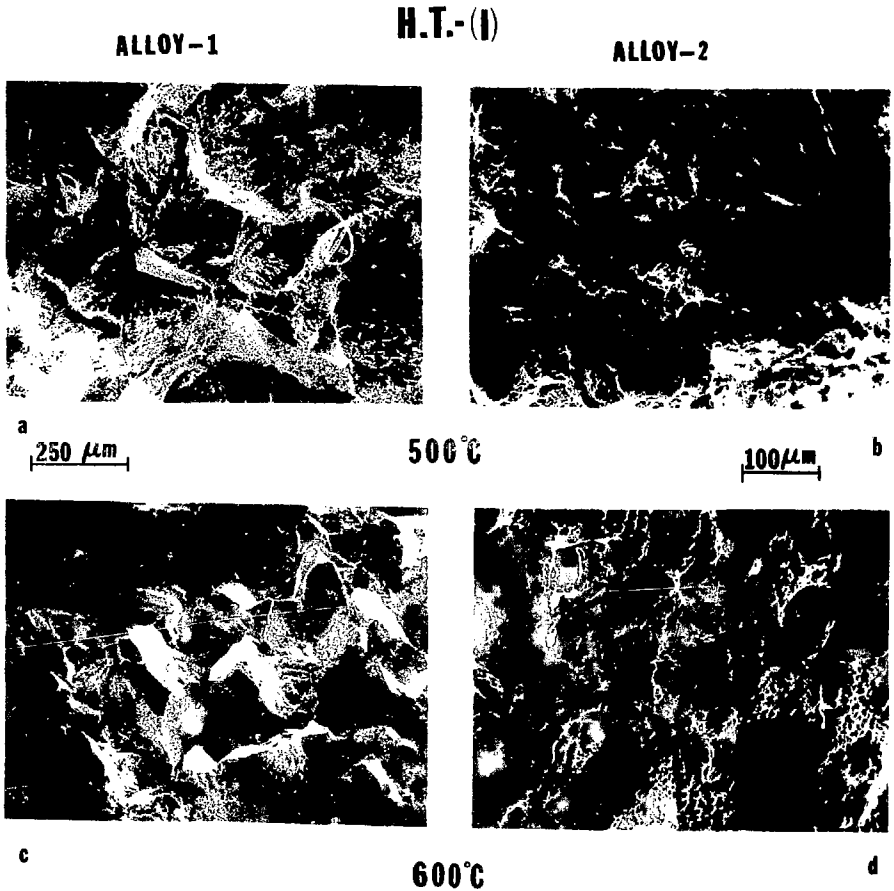

XBB 780-13907

Fig. 34

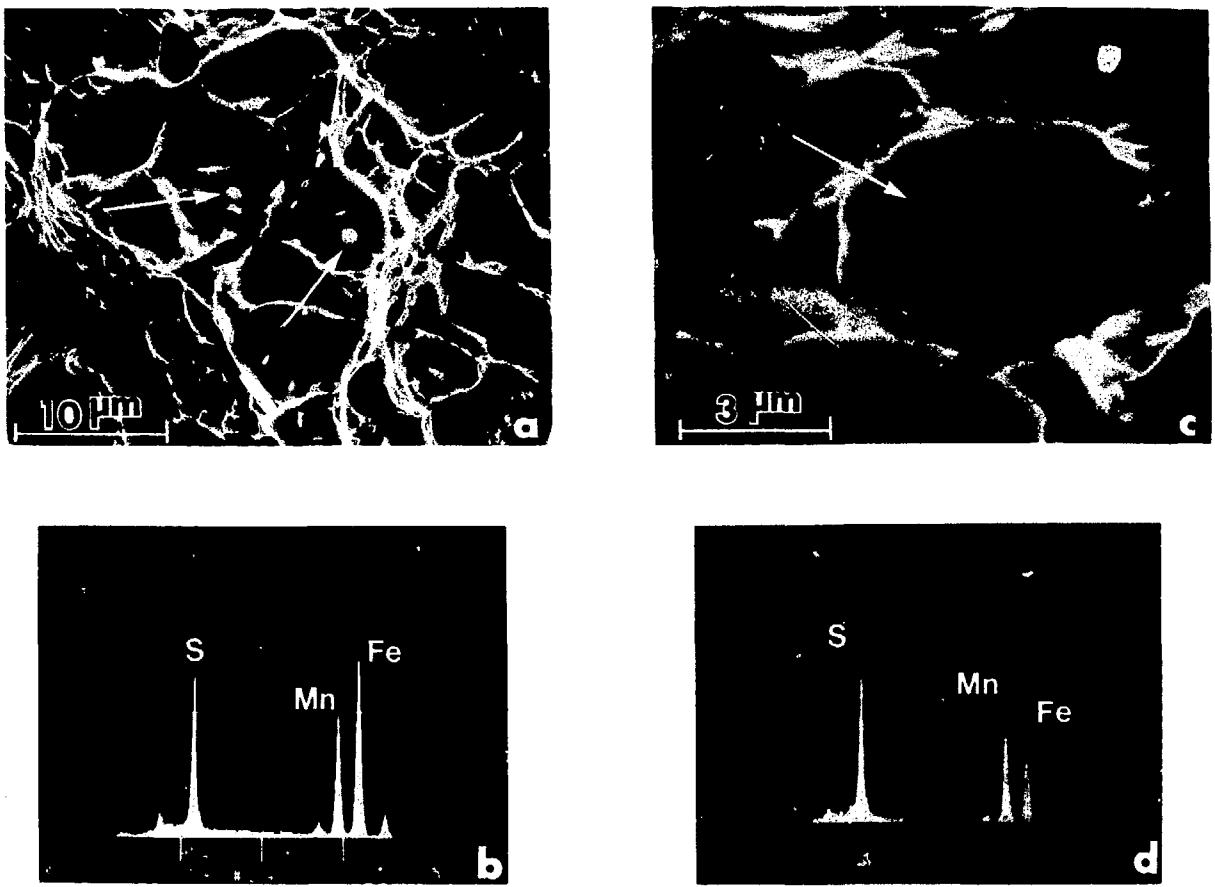

XBB 794-05473

Fig. 35

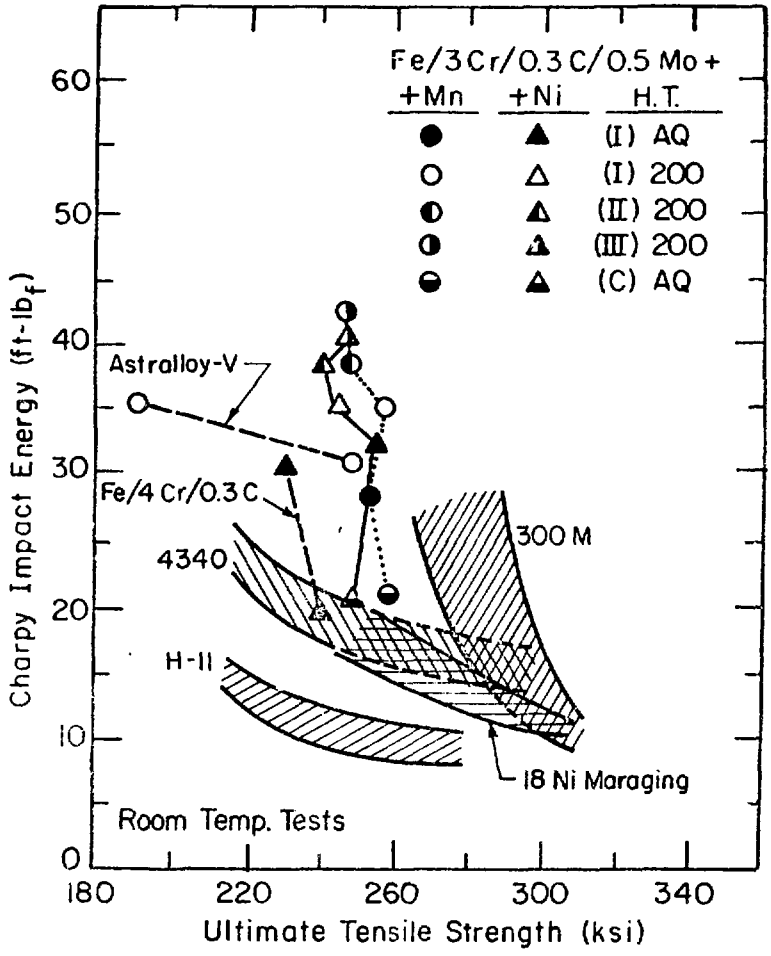

XBL 795-6240

Fig. 36a

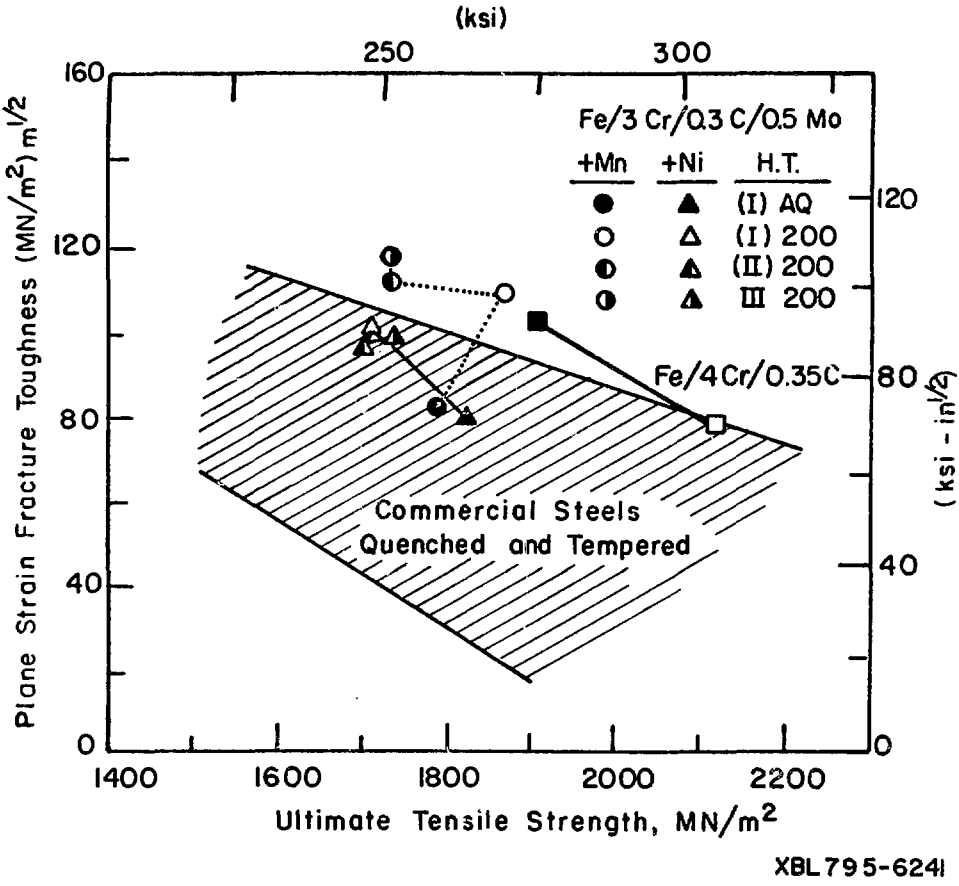
(ksi)
250
300
160
120
80
40
0
Fe/3 Cr/0.3 C/0.5 Mo
+Mn
+Ni
H.T.
(I) AQ
(I) 200
(II) 200
III 200
Fe/4Cr/0.35C
Commercial Steels
Quenched and Tempered
Plane Strain Fracture Toughness (MN/m²) m^1/2
(ksi - in^1/2)
120
80
40
0
1400
1600
1800
2000
2200
Ultimate Tensile Strength, MN/m²
XBL795-6241

Fig. 36b